Dynamic changes in the urine proteome of tumor-bearing mouse models of B16 melanoma and RM-1 prostate cancer

Lujun Li[1], Xuanzhen Pan[1], Yongtao Liu[1], Ting Wang[1,2], Youhe Gao[1]

1. Department of Biochemistry and Molecular Biology, Gene Engineering Drug and Biotechnology Beijing Key Laboratory, Beijing Normal University, Beijing 100875, China

2. Beijing Jingshan School Daxing Experimental School, Beijing 100076, China

Corresponding author: Youhe Gao

E-mail: gaoyouhe@bnu.edu.cn

This work was supported by National Key Research and Development Program of China (2018YFC0910202, 2016YFC1306300), the Fundamental Research Funds for the Central Universities (2020KJZX002), Beijing Natural Science Foundation (7172076), Beijing Cooperative Construction Project (110651103), Beijing Normal University (11100704), and Peking Union Medical College Hospital (2016-2.27).

Abstract: Urine can accumulate changes and reflect early physiological and pathological changes of various diseases, such as tumors. Therefore, urine is an ideal source for identification of early biomarkers. In this study, melanoma and prostate cancer-bearing mouse models were established by subcutaneous injection of B16 and RM-1 cells, respectively. Urine samples were collected at four time points during tumor growth. Based on data-independent acquisition (DIA) technology, liquid chromatography-tandem mass spectrometry (LC-MS/MS) was used for quantitative analysis. Compared with those before the injection of B16 cells, 38 human homologous differential proteins were identified, and 18 proteins were reported to be related to melanoma. Before the tumor was visible, there were 4 differential proteins, and all were reported to be related to melanoma. Compared with that before the injection of RM-1 cells, a total of 14 human homologous differential proteins were identified, and 9 proteins were reported to be associated with prostate cancer. Before the tumor was palpable, 9 proteins showed significant differences. There were significant differences between the two tumor-bearing models. Through the above experiments and analysis, we found that the urine proteome can reflect the changes in the development and provide early biomarkers of the two tumors and provide clues for the early clinical diagnosis of these diseases.

Key words: Urine proteome, Melanoma, Prostate cancer, Biomarker

Skin melanoma is one of the most common cancers in the world[1]. Melanoma is produced by the malignant transformation of melanocytes. This disease can occur in any part of the skin and mucous membranes. Melanoma easily metastasizes and is highly invasive and malignant, leading to high mortality. The diagnosis of melanoma is based on a combination of clinical and pathological techniques, including physical examination, histopathological examination and imaging

examination. However, due to its variable histological morphology, with little or even no visible pigment, it is difficult to diagnose patients in the early stage and distinguish this condition from benign nevus in the clinic, which makes its early diagnosis difficult[2]. Early treatment of melanoma is mainly surgery, and advanced treatment includes chemotherapy, targeted therapy and immunotherapy. Compared with chemotherapy alone, targeted therapy and immunotherapy have significantly improved the survival rate of patients with advanced melanoma, but these two therapies are usually limited by the drug resistance rate and are not universally applicable[3, 4]. The absolute survival rate of patients is still very low[5]. The 5-year survival rates of skin melanoma at stage I to IV are 97% (stage IA), 84% (stage IB), 68%, 55%, and 17%[6]. Therefore, early diagnosis can lead to early treatment and improve the survival rate of patients.

Prostate cancer is one of the most common malignant tumors in men. In Europe and America, the incidence rate is highest among those of all cancers in males. The mortality rate is second only to that of lung cancer, ranking second for malignant tumors in males[7]. The incidence rate and mortality rate of the Asian population have also shown an increasing trend[8]. Prostate cancer grows slowly, has no clinical symptoms in the early stage, is easily confused with benign hyperplasia, and develops rapidly in the later stage, leading to malignant metastasis[9, 10]. Early detection and treatment can significantly improve the survival rate of prostate cancer[11]. Existing diagnostic methods, such as digital rectal examination (DRE), transrectal ultrasound (TRUS), serum PSA, and puncture biopsy, cannot truly achieve high sensitivity and specificity. Therefore, it is necessary to find a new method for the early diagnosis of prostate cancer.

Biomarkers are a class of indicators that can objectively reflect normal physiological and pathological processes[12]. From a clinical perspective, biomarkers can help with the monitoring, prediction and diagnosis of multifactorial diseases at different stages[13]. Blood is a relatively stable system. As the disease progresses, when the blood reaches the critical point of compensation, loss of compensation is observed. Before reaching the critical point of decompensation, changes caused by the disease are eliminated by the blood. In this process, one of the most important environments for metabolic waste is urine. Therefore, sensitive early biomarkers are more likely found in the urine than the blood[14].

Urine is susceptible to gender, age, diet and other factors[15]. The use of animal models with controllable living conditions and clear genetic backgrounds can not only avoid the interference of the above factors but can also continuously monitor the course of disease. Previous studies have shown that urine can sensitively reflect the changes in tumor cells in animal models[16, 17] To explore the effects of the occurrence and development of melanoma and prostate cancer on the urine proteome, we established tumor-bearing mouse models by subcutaneously injecting B16 and RM-

1 tumor cells, respectively. Urine samples were collected at four time points corresponding to tumorigenesis and development, and the urine proteome was analyzed by liquid chromatography-tandem mass spectrometry (LC-MS/MS) based on data-independent acquisition (DIA) technology. The above results provide valuable clues for the early clinical diagnosis of melanoma and prostate cancer in the future.

1 Materials and methods

1.1 Cell lines and reagents

B16 mouse melanoma cells and RM-1 mouse prostate cancer cells were purchased from the Cell Bank of the Chinese Academy of Sciences. The cells were cultured in RPMI-1640 (Corning) containing 10% fetal bovine serum (Gibco) at 37℃ and 5% CO_2.

1.2 Experimental animals and model establishment

Seven-week-old male C57BL/6 mice were purchased from Beijing Vital River Laboratory Animal Technology Co., Ltd. The animal license is SCXK (Beijing) 2016-0006. Animal procedures were approved by the Institute of Basic Medical Sciences Animal Ethics Committee, Peking Union Medical College (ID: ACUC-A02-2014-008). All animals were housed in a standard environment with a 12-h light-dark cycle under controlled indoor temperature (22 ± 2°C) and humidity (65–70%).

The methods of subcutaneous injection of B16[18-20] and RM-1[21, 22] cells to establish the tumor-bearing mouse model are as follows: the number of living cells was more than 95% as calculated by trypan blue staining. (1) The melanoma-bearing mouse model was established by subcutaneous injection of 0.1 mL of B16 cells ($1.8x10^5$) in the right hind limb of the mice (n = 8). (2) The model of prostate cancer-bearing mice was established by subcutaneous injection of 0.1 mL RM-1 cells ($1.9x10^4$) into the right hind limb of mice (n = 4). This experiment used an autocontrol, the urine collected before the injection of tumor cells was used as the control group, the time was recorded as day 0, and the time of subcutaneous injection of the tumor cells was recorded as day 1.

1.3 Urine collection and sample preparation

Urine samples of the B16 tumor-bearing mice on days 0, 4, 7 and 14 and the RM-1 tumor-bearing mice on days 0, 7, 15 and 22 were collected. The mice were placed in a metabolic cage

alone overnight (12 h) to collect urine samples. During urine collection, no food was provided, and free drinking water was available to avoid urine pollution.

The collected urine was centrifuged at 4℃ and 3000 × g for 10 min to remove the cells and pellets. The supernatant was stored at -80℃. Prior to urine protein extraction, the urine samples were centrifuged at 4℃ and 12000 × g for 10 min to remove cell debris. Four volumes of precooled ethanol were used, and the supernatant was precipitated at 4℃ for 12 h. The above samples were centrifuged at 4℃ and 12000 × g for 10 min. The pellet was resuspended in lysate (8 mol/L urea, 2 mol/L thiourea, 25 mmol/L DTT and 50 mmol/L Tris). The Bradford method was used to determine the protein concentration.

Filter-aided sample preparation (FASP)[23] was used for membrane-assisted enzymolysis of urine proteins. One hundred micrograms of protein was loaded onto 10-kD cutoff filter devices (Pall, Port Washington, NY). The samples were washed sequentially with UA (8 mol/L urea, 0.1 mol/L Tris-HCl, pH 8.5) and 50 mmol/L NH_4HCO_3. Then, 20 mmol/L DTT was added to reduce the protein (37℃, 1 h), and 50 mmol/L IAA was reacted in the dark for 30 min to alkylate the proteins. The proteins were digested with trypsin (Trypsin Gold, Promega, Fitchburg, WI, USA) (enzyme-to-protein ratio of 1:50) for 14 h at 37°C. The peptides were collected and desalted on Oasis HLB cartridges (Waters, Milford, MA) and then dried by vacuum evaporation (Thermo Fisher Scientific, Bremen, Germany) and stored at -80℃.

Pooled peptides were fractionated by a high-pH reversed-phase peptide fractionation kit (84868, Thermo Fisher, USA) according to the manufacturer's instructions. The peptide samples were eluted with a gradient of increasing acetonitrile concentration. A total of 10 fractions were collected: the flow-through fraction, wash fraction and 8 step gradient sample fractions. The fractionated samples were dried completely and resuspended in 20 μL of 0.1% formic acid.

1.4 LC-MS/MS analysis

1.4.1 DDA-MS

LC-MS/MS data acquisition was performed on a Fusion Lumos mass spectrometer (Thermo Scientific, Germany) coupled with an EASY-nLC 1200 high-performance liquid chromatography system (Thermo Scientific, Germany). For both DDA-MS and DIA-MS modes, the same LC settings were used for stability of the retention time. The digested peptides were dissolved in 0.1% formic acid and loaded on a trap column (75 μm × 2 cm, 3 μm, C18, 100 A˚), and the eluent was transferred to a reversed-phase analytical column (50 μm × 250 mm, 2 μm, C18, 100 A˚) with an elution gradient of 5-30% phase B (79.9% acetonitrile, 0.1% formic acid, flow rate of 0.5 μL/min) for 90 min. For fully automated and sensitive signal processing, the calibration kit (iRT kit,

Biognosys, Switzerland) was spiked at a concentration of 1:20 v/v in all samples.

For the generation of the spectral library, 10 peptide fractions were analyzed in DDA-MS mode. The parameters were set as follows: the full scan was acquired from 350 to 1 550 m/z at 60 000, the cycle time was set to 3 s (top speed mode), the auto gain control (AGC) was set to 1e6 and the maximum injection time was set to 50 ms. The MS/MS scans were acquired in the Orbitrap at a resolution of 15000 with an isolation window of 2 Da and collision energy at 32% (HCD). The AGC target was set to 5e4, and the maximum injection time was 30 ms.

1.4.2 DIA-MS

For the DIA-MS method, 48 individual samples were analyzed in DIA mode. The parameters were set as follows: the full scan was acquired from 350 to 1 550 m/z at 60000, followed by DIA scans with a resolution of 30000, HCD collision energy of 32%, AGC target of 1e6 and maximal injection time of 50 ms. Thirty-six variable isolation windows were developed, and the calculation method of the windows was as follows: the DDA search results were sorted according to the number of identified peptide segments by m/z and divided into 36 groups. The m/z range of each group is the window width for collecting DIA data.

1.5 Data analysis

For generation of the spectral library, the ten fractions' raw data files acquired by the DDA mode were processed using Proteome Discoverer (version 2.3, Thermo Scientific, Germany) with the SwissProt mouse database (released in May 2019, containing 17016 sequences) appended with the iRT peptide sequences. The search parameters were as follows: parent ion mass tolerance, 10 ppm; fragment ion mass tolerance, 0.02 Da; fixed modifications, carbamidomethylated cysteine (+58.00 Da); and variable modifications, oxidized methionine (+15.995 Da). Other settings included the default parameters. The applied false discovery rate (FDR) cutoff was 0.01 at the protein level. The results were then imported to Spectronaut™ Pulsar (Biognosys, Switzerland) software to generate the spectral library: 798 proteins and 28356 fragments.

The DIA-MS raw files were imported to Spectronaut™ Pulsar with the default settings. Quantitative analysis was based on the peak areas of all fragment ions for MS2. Each protein was identified with at least two specific peptides and a Q value < 0.01. The screening criteria for differential proteins were as follows: fold change of protein abundance > 1.5, p value < 0.01 by t-tests.

1.6 Functional enrichment analysis

The online database DAVID 6.8 (https://david.ncifcrf.gov/) was used to perform the functional annotation of the differential proteins, including molecular function, cell component and biological process. Pathway analysis of differential proteins was performed using IPA software (Ingenuity Systems, Mountain View, CA, USA).

2 Results and Discussion

2.1 Characterization of the tumor-bearing mice

After the tumor cells were inoculated, the growth of subcutaneous tumor masses in the tumor-bearing mice was observed daily.

From day 7, small black and untouchable tumor masses were observed in the B16 melanoma-bearing mice, and the tumor masses grew gradually. The mice were killed on the 15th day, and the tumor masses were weighed. The average tumor mass of the 8 tumor-bearing mice was 0.68 ± 0.15 g. The tumor tissue was stained with hematoxylin and eosin (H&E) for pathological examination, and many tumor cells were observed in the tumor mass (Figure 1).

From day 15, small palpable tumor masses were observed in the RM-1 prostate cancer-bearing mice, and the tumor masses grew gradually. The mice were killed on the 23rd day, and the tumor masses were weighed. The average tumor mass of 4 tumor-bearing mice was 0.90 ± 0.13 g. Tumor tissue was stained with hematoxylin and eosin (H&E) for pathological examination, and many tumor cells were observed in the tumor mass (Figure 2).

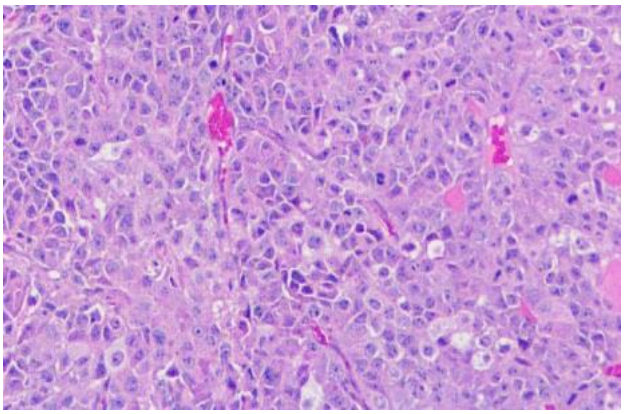

Figure 1 H&E staining of tumors in the B16 tumor-bearing mice (100 ×)

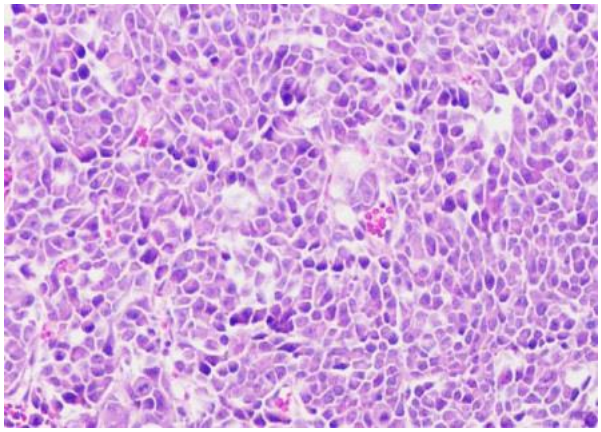

Figure 2 H&E staining of tumors in the RM-1 tumor-bearing mice (100 ×)

2.2 Urine proteome changes

Randomly grouped samples at each time point according to different combinations of fold changes (1.5 or 2) and p values (0.01 or 0.05) were used to calculate the average number of differential proteins under different screening conditions. This value was compared with the correct number of differential proteins under this screening condition, and this ratio can be approximated as a false positive rate. The lower the false positive rate, the higher the reliability is. In addition, since the true positive differential proteins are included in the results of all random groupings, the ratio of the approximate false positive rate should be slightly higher than the actual false positive rate (Table 1, Table 2).

Based on the analysis of the random data of two tumor-bearing models, the screening criteria of the differential proteins we selected were as follows: fold change > 1.5, p value < 0.01. Furthermore, the UniProt database was used to match the human homologous proteins corresponding to these proteins for further analysis.

The differential proteins of the two tumor models at different time points changed significantly with tumor growth, suggesting that the urine proteome has the potential to reflect the occurrence and development of tumors.

Table 1 Random grouping results of the B16 tumor-bearing mice under different combinations of p values and fold changes

	D4	D7	D14
1.5，0.05	11.5/26，0.44	13.3/28，0.48	14.1/73，0.19
2，0.05	4.4/4，1.1	4.8/8，0.6	5.6/35，0.16
1.5，0.01	2.3/7，0.33	2.5/12，0.21	2.7/42，0.06

2，0.01	0.8/2，0.4	0.9/4，0.23	1.2/22，0.05

Note: expressed in the form of "average differential protein number/due differential protein number, ratio of the two"

Table 2 Random grouping results of the RM-1 tumor-bearing mice under different combinations of p values and fold changes

	D7	D15	D22
1.5，0.05	10.9/27，0.4	10.5/13，0.81	9.8/31，0.32
2，0.05	5.3/12，0.44	5.7/5，1.14	4.9/17，0.29
1.5，0.01	2.2/9，0.24	1.8/1，1.8	2.0/11，0.18
2，0.01	1.1/2，0.55	1.1/1，1.11	1.2/6，0.2

Note: expressed in the form of "average differential protein number/due differential protein number, ratio of the two"

2.2.1 B16 melanoma-bearing mice

By DIA quantitative analysis, a total of 532 proteins were identified. Thirty-eight human homologous differential proteins were identified compared with those on Day 0. On Day 4, there were 4 differential proteins, of which 3 were upregulated and 1 was downregulated. On Day 7, there were 7 differential proteins, of which 3 were upregulated and 4 were downregulated. On Day 14, there were 29 differential proteins, of which 21 were upregulated and 8 were downregulated. There were no continuously changing proteins (Figure 3, Table 3).

On Day 4, the tumor was not yet visible, and a total of 4 differential proteins were significantly changed, all of which were reported to be related to melanoma. For example, (1) Osteopontin acts as a cytokine and is involved in type I immune responses. Osteopontin-dependent autocrine/paracrine signaling pathways are associated with metastatic melanoma[24], and the protein is involved in cell signaling that regulates tumor progression and metastasis[25]. (2) Carbonic anhydrase 1 participates in interleukin 12-mediated signaling pathways, while Carbonic anhydrase IX inhibitors can increase the sensitivity to chemotherapy and promote the apoptosis of melanoma cells[26]. (3) Mucin-13 is a cell surface glycoprotein that is abnormally expressed in various epithelial cancers. Serum mucin 13 is elevated in 70% of active skin melanoma patients (except for uveal melanoma)[27]. (4) Alpha-cardiac actin is involved in various types of cell movements. Cancer cells need to undergo continuous actin cytoskeleton remodeling to adapt to environmental mechanical stimuli, thereby promoting their survival, migration and metastasis[28, 29]. In addition, β-actin was found to be abnormally expressed in diseases such as melanoma,

colorectal cancer, gastric cancer, pancreatic cancer, prostate cancer, and ovarian cancer[30].

On Day 7, the tumor was visible, and a total of 7 differential proteins changed significantly, of which 5 were reported to be associated with melanoma. For example, (1) SPINT2, a proteolytic inhibitor of Hepatocyte growth factor activator, plays an important role in inhibiting the progression of malignant melanoma[31]; (2) downregulation of Insulin-like growth factor-binding protein 4 may be a step in the development of primary melanoma to metastatic melanoma[32]; (3) Peroxiredoxin-3 plays a protective role in cell antioxidant stress. The expression of this protein in the cytoplasm of stromal fibroblasts is related to melanoma-specific survival[33]. (4) Tripeptidyl-peptidase 1 (TPP1) was identified, and POT1-A532P is a POT1 mutation associated with melanoma, which can weaken the interaction of TPP1-POT1[34].

On Day 14, a total of 29 differential proteins were significantly changed, of which 10 were reported to be associated with melanoma. For example, (1) Copper transport protein ATOX1 may be an important cellular antioxidant. The interaction between the anticancer drug cisplatin and the copper transporter ATOX occurs in human melanoma cells[35]. (2) Galectin-3-binding protein has scavenger receptor activity, promotes integrin-mediated cell adhesion, and may stimulate host defense against viruses and tumor cells. Significant upregulation in serum or tumor tissue correlates with poor clinical outcomes in melanoma patients[36-38], and its inhibitors have potential as antimetastatic cancer drugs[39]. (3) Prothrombin plays a role in blood homeostasis, inflammation, and wound healing. Its complex is involved in the production of thrombin in B16F10 melanoma cells[40]; (4) Prostaglandin-H2 D-isomerase may play an important role in the progression of uveal melanoma[41]; (5) Intercellular adhesion molecule 1 is involved in the acute inflammatory response to antigen stimulation. The upregulation of this protein is the key to the lymphatic proliferation of melanoma[42]; (6) Cell adhesion molecule 4 is involved in intercellular adhesion and may have cancer suppressive activity[43]. Melanoma cell adhesion molecule (Mel-CAM) has been shown to be a sensitive marker for epithelioid melanoma [44]; (7) Nuclear transport factor 2 plays an important role in the transport process mediated by the cargo receptor and plays a more general role indirectly. RanBP3 (a potential target for human melanoma therapeutic intervention) regulates melanoma cell proliferation through selective control of nuclear export[45]; (8) Eukaryotic translation initiation factor 6 modulates cell cycle progression and global translation of pre-B cells, and its activation seems to be rate-limiting in tumorigenesis and tumor growth[46] and is positively correlated with tumor tissue content in patients with metastatic melanoma[47]; (9) Disintegrin and metalloproteinase domain-containing protein 9 cleaves and releases many molecules that play important roles in tumorigenesis and angiogenesis and are potential tumor targets[48]. The protein is specifically expressed in stromal fibroblasts and can regulate the proliferation and apoptosis of

melanoma cells in vitro and in vivo[49], and its expression is helpful for melanoma invasion[50]; (10) For Neutral ceramidase, acid ceramidase expression regulates the sensitivity of A375 melanoma cells to dacarbazine (the drug of choice for metastatic melanoma)[51].

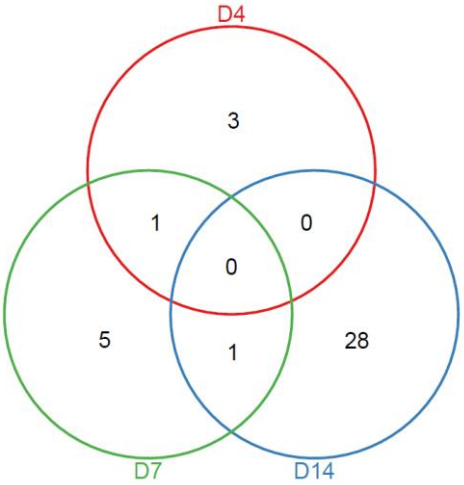

Figure 3 Venn diagram of differential proteins at different stages in the B16 tumor-bearing mice

Table 3 Differential proteins in the B16 tumor-bearing mice

UniProt ID	Protein name	Fold change			PubMed
		D4	D7	D14	Melanoma
P10451	Osteopontin	1.88			PMID: 28158294
P00915	Carbonic anhydrase 1	1.62			PMID: 30362384
Q9H3R2	Mucin-13	2.24			PMID: 29768245
P68032	Alpha-cardiac actin	0.42	0.46		PMID: 23266771
O14773	Tripeptidyl-peptidase 1		0.65		PMID: 26365187
P30048	Peroxiredoxin-3		1.83		PMID: 25627040
P22692	Insulin-like growth factor-binding protein 4		0.49		PMID: 19025658
P55017	Solute carrier family 12 member 3		1.76	2.00	
Q14393	Growth arrest-specific protein 6		1.51		
Q04756	Hepatocyte growth factor activator		0.66		PMID: 25910030
O00244	Copper transport protein ATOX1			2.42	PMID: 23988033
P41222	Prostaglandin-H2 D-isomerase			3.46	PMID: 25938039
Q99519	Sialidase-1			0.52	
P56537	Eukaryotic translation initiation factor 6			5.95	PMID: 28445515 PMID: 16850525
Q0KKI6	Immunoglobulin kappa constant			1.52	

P04003	C4b-binding protein	2.64	
P05362	Intercellular adhesion molecule 1	0.56	PMID: 29245925
P00734	Prothrombin	1.73	PMID: 15567463
P26927	Hepatocyte growth factor-like protein	1.93	
P61970	Nuclear transport factor 2	4.26	PMID: 26763446
P99999	Cytochrome c, somatic	3.14	
P68371	Tubulin beta-4B chain	0.47	
P78310	CVB3-binding protein	1.64	
			PMID: 30821848
		1.64	PMID: 30553852
Q08380	Galectin-3-binding protein		PMID: 26160844
Q9P1F3	Costars family protein ABRACL	4.46	
Q86UQ4	ATP-binding cassette sub-family A member 13	0.66	
P02763	Alpha-1-acid glycoprotein 1	0.66	
Q13443	Disintegrin and metalloproteinase domain-containing protein 9	2.20	PMID: 22622419 PMID: 21135106
Q9NPH3	Interleukin-1 receptor accessory protein	0.50	
Q8NFZ8	Cell adhesion molecule 4	1.91	PMID: 11145252
Q9BZP6	Acidic mammalian chitinase	0.51	
P02787	Transferrin	0.46	
O95336	6-phosphogluconolactonase	2.21	
Q9BRT3	Migration and invasion enhancer 1	5.14	
O43169	Cytochrome b5 type B	3.24	
Q9NRX4	14 kDa phosphohistidine phosphatase	5.04	
Q9NR71	Neutral ceramidase	2.08	PMID: 21700700
A8MVZ5	Butyrophilin-like protein 10	1.79	

2.2.2 RM-1 prostate cancer-bearing mice

By DIA quantitative analysis, a total of 406 proteins were identified. Compared with those on Day 0, 14 human homologous differential proteins were identified. On Day 7, there were 9 differential proteins, of which 6 were upregulated and 3 were downregulated. On Day 15, there was no differential protein. On Day 22, there were 6 differential proteins, of which 3 were upregulated and 3 were downregulated. Transferrin changed continuously at the two time points (Figure 4, Table 4).

On Day 7, the tumor was not yet palpable, and a total of 9 differential proteins changed

significantly, of which 6 were reported to be associated with prostate cancer. For example, (1) Clusterin is upregulated in prostate cancer solid tumors [52], and the intracellular level in patients is related to the Gleason score[53]; (2) Transferrin is an iron-binding transporter and an effective mitogen for prostate cancer[54, 55], and upregulation of Transferrin is often associated with increased adhesion, invasion, and metastasis[56]. For example, Transferrin receptors are direct MYC target genes, and MYC oncogenes are important mediators of tumor initiation and progression in prostate cancer[57]. Studies have shown that the Transferrin concentration in the prostate fluid of prostate cancer patients is significantly higher than that of patients with benign prostatic hyperplasia and normal controls[58]. Compared with the healthy controls, 18/22 prostate cancer patients had a significant increase in Transferrin in their urine[59]. (3) Voltage-dependent anion-selective channel protein 1 participates in the formation of channels across the mitochondrial outer membrane and plasma membrane. The mRNA expression of its genes is significantly increased in prostate cancer tissues [60]. Zinc and p53 destroy the mitochondrial binding of hexokinase 2, which has dual metabolic and apoptotic functions in prostate cancer cells through phosphorylation of voltage-dependent anion selective channel protein 1[61]; (4) Voltage-dependent anion-selective channel protein 3 participates in the formation of a channel across the outer mitochondrial membrane, and there is no significant difference in the mRNA expression of its genes in prostate cancer tissues[60]; (5) Cartilage oligomeric matrix protein promotes the progression of prostate cancer by enhancing infiltration and disrupting intracellular calcium homeostasis[62]; this protein in patients with osteoarthritis is independently associated with metastatic disease of prostate cancer [63]. Studies have shown that prostate cancer cells tend to show bone metastasis, which is the main cause of morbidity and mortality in prostate cancer patients[64]. (6) Beta-2-glycoprotein 1 may prevent activation of the intrinsic coagulation cascade by binding to phospholipids on the surface of damaged cells. Human phosphatidylserine-targeting antibody fragments can be used as highly specific tumor imaging agents by interacting with Beta-2-glycoprotein 1 to form high-affinity complexes. This study has been verified in nude mice with subcutaneous or in situ human prostate tumors[65].

On Day 15, the tumor was just palpable, and there was no significant change in protein.

On Day 22, a total of 6 differential proteins were significantly changed, of which 4 were reported to be associated with prostate cancer. For example, (1) Progranulin is a growth factor involved in inflammation[66], tumorigenesis and development[67] and may play a key role in the progression of prostate cancer, promoting movement and proliferation [68]; (2) Growth arrest-specific protein 1 is a growth inhibitory protein that participates in growth inhibition and prevents entry into S phase [69], and 8 gene tags including this gene have the potential to diagnose prostate

cancer[70]; (3) Myosin light chain kinase in smooth muscle participates in inflammatory response, promotes cell migration and tumor metastasis and is a new downstream target of the androgen signaling pathway in prostate cells. Androgen can downregulate the expression of myosin light chain kinase in LNCaP human prostate cancer cell lines[71], and circRNA-myosin light chain kinase can promote the progression of prostate cancer[72].

At present, it is not clear why this phenomenon occurred on Day 15 without differential proteins. By reviewing the original data, we found that the condition that limited the screening of differential proteins was mainly the p value. At this time point, there were only five human homologous differential proteins under the screening condition of "fold change greater than 1.5 times and p value less than 0.05": Acid sphingomyelinase-like phosphodiesterase 3b, Acid sphingomyelinase-like phosphodiesterase 3a, Galectin-3-binding protein, Adhesion G-protein coupled receptor G1, and Cartilage oligomeric matrix protein. These five proteins are mainly involved in lipid metabolism, cell adhesion, and the immune response and participate in various signal transduction pathways, which are involved in tumorigenesis; that is, when the body fights tumor cells, tumor cells prepare for subsequent infinite growth, invasion and metastasis.

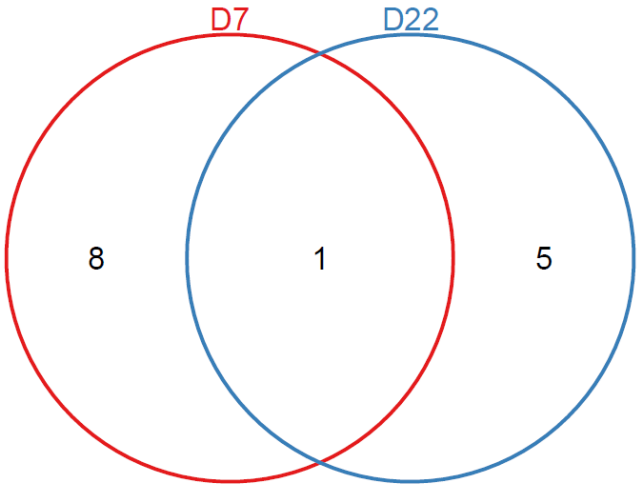

Figure 4 Venn diagram of differential proteins at different stages in the RM-1 tumor-bearing mice

Table 4 Differential proteins in the RM-1 tumor-bearing mice

UniProt ID	Protein name	Fold change		PubMed
		D7	D22	Prostate cancer
P02749	Beta-2-glycoprotein 1	0.49		PMID: 24367699
P10909	Clusterin	1.51		PMID: 9815554 PMID: 26313417
Q9Y277	Voltage-dependent anion-selective channel	1.70		PMID: 25177836

	protein 3			
	Voltage-dependent anion-selective channel			PMID: 30528266
P21796	protein 1	2.01		PMID: 25177836
Q92896	Golgi apparatus protein 1	1.62		
P02787				PMID: 2433078 PMID: 7029542 PMID: 8989919 PMID: 28592703 PMID: 15619922
	Transferrin	0.64	0.58	PMID: 29135121
P04066	Tissue alpha-L-fucosidase	1.69		
P49747	Cartilage oligomeric matrix protein	0.52		PMID: 29228690 PMID: 31413818
O95497	Pantetheinase	1.69		
P28799	Progranulin		1.86	PMID: 25365768
O14745	Na(+)/H(+) exchange regulatory cofactor NHE-RF1		0.35	
P10253	Lysosomal alpha-glucosidase		1.85	
P54826	Growth arrest-specific protein 1		1.81	PMID: 18974881 PMID: 1505026 PMID: 29798970
Q15746	Myosin light chain kinase, smooth muscle		0.54	PMID: 19429448

2.2.3 Comparison of the differential proteins in the urine of the B16 melanoma, RM-1 prostate cancer and Walker 256 tumor-bearing models

In total, 37 and 13 unique differential proteins were identified (Figure 5) by comparing B16 melanoma and RM-1 prostate cancer in the tumor-bearing mice, and the only overlapping protein was Transferrin. It has been reported that Transferrin is widely used as a tumor-targeting ligand for anticancer drugs because the transferrin receptor is overexpressed on the surface of various rapidly growing cancer cells, which have an affinity for Transferrin that is 10-100 times higher than that of normal cells, thus providing an effective means of targeting cancer cells for treatment[73, 74]. Of the above unique differential proteins, 17/37 have been reported to be related to melanoma, and 8/13 have been reported to be related to prostate cancer; that is, the urine proteome can reflect the

differences in the production of different tumors in the same animals and at the same site. Presumably, the reason for the substantial difference in the number of proteins between the two models is that the subcutaneous tumor-bearing model of melanoma is closer to the in situ model, which has a greater impact on the urine proteome.

At $p < 0.01$, comparing homologous proteins among the two tumor models of B16 and RM-1 model and laboratory research on a Walker 256 (W256) carcinosarcoma model[16], we found distinctive differential proteins (31, 12, and 49), all of which comprised more than half of each differential protein type. There was no common variation in the differential proteins in the three tumor-bearing animal models, but there were common differences between every two models (Figure 6). Overlapping proteins are 6-phosphate glucose acid esterase, intercellular adhesion molecule 1, nuclear transport factor 2, carbonic anhydrase 1, galactosyl lectin-3-binding protein, lysosome alpha glycosidase enzymes, transferrin, and acidic mammalian chitinase. The molecular functions and biological processes involved in the above 8 proteins are mostly related to energy metabolism, material transport, inflammatory response and immune response. To some extent, the results of comparisons showed that there was a certain similarity in the growth of different tumors at the same site, but the difference reflected in the urine proteomes was much greater than the similarity; that is, the urine proteome was sensitive enough to reflect the changes of different tumors.

A comparison was performed with the differential proteins obtained from three tumor-bearing animal models (B16, RM-1 and W256) in the early stage (before the tumor was detectable) (Figure 7). We found that the three tumor-bearing animal models had no differential proteins with common changes, and there were no differential proteins between every two models; that is, urine proteomics is sensitive enough to reflect changes in the growth of different tumors, even before the tumor is detectable.

The above results suggest that urine has potential for early diagnosis, differentiation of different tumor types and development.

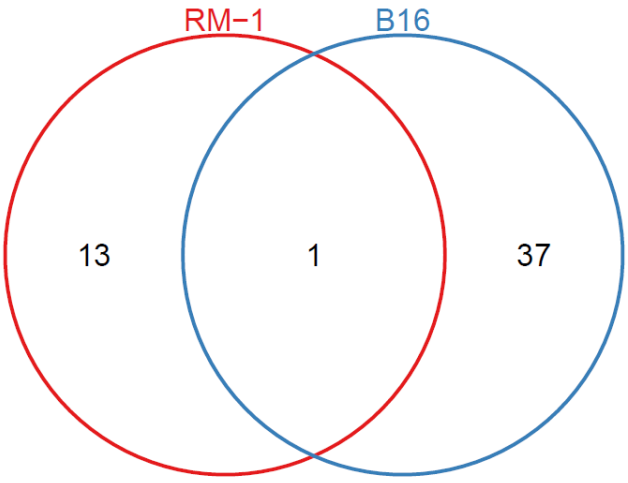

Figure 5 Venn diagram of differential proteins between the B16 and RM-1 tumor-bearing models

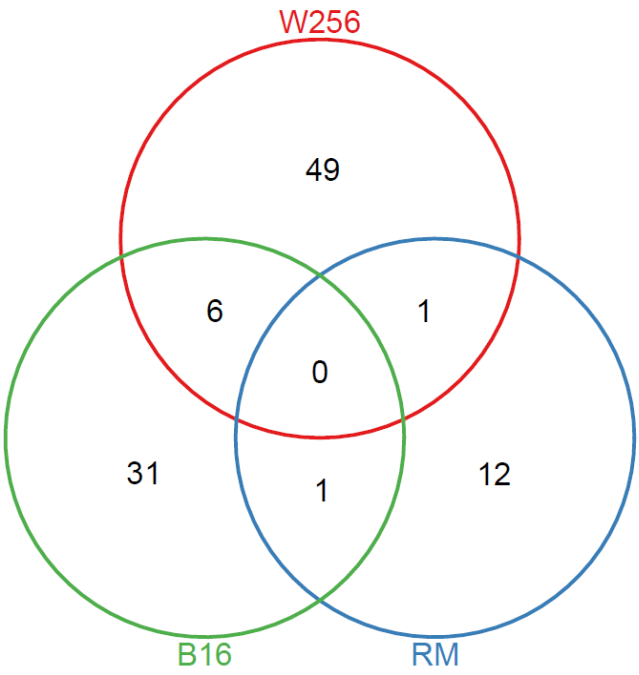

Figure 6 Venn diagram of differential proteins among the B16, RM-1 and W256 tumor-bearing models

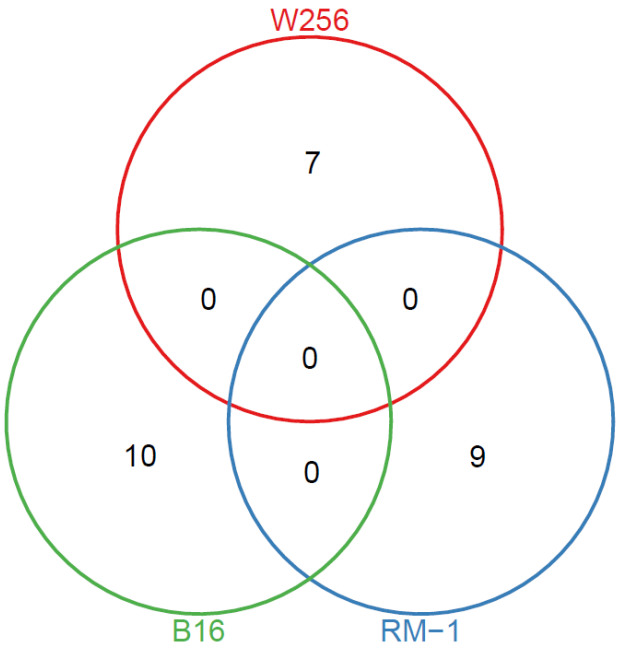

Figure 7 Venn diagram of early differential proteins among the B16, RM-1 and W256 tumor-bearing models

2.3 Functional enrichment analysis of the differential proteins

DAVID was used to annotate the function of the differential proteins, showing the biological process, cell composition and molecular function of these proteins at each time point. Pathway analysis of the proteins was performed by using IPA.

In general, the more stringent the screening conditions are, the lower the average differential protein number, the number of expected differential proteins, and the false positive rate are. However, the more stringent the screening conditions are, the fewer differential proteins will be obtained, and the false-negative proteins will be screened out. When the differential proteins obtained under strict screening conditions are used for biological function analysis, there will be less relevant information. Therefore, in the biological function analysis of the differential proteins, this experiment mainly analyzed the proteins screened with the condition of "fold change > 1.5, p value < 0.01", which supplemented the proteins screened under the condition of "fold change > 1.5, p value < 0.05", for reference.

2.3.1 B16 melanoma-bearing mice

According to the analysis of biological processes, apoptotic processes were shown on Day 7, and cell adhesion and inflammatory processes were shown on Day 14, which were related to tumor invasion and metastasis (Figure 8A). Analysis of cell composition revealed that the differential proteins were secreted proteins, mostly from the extracellular matrix, cell surface and membrane (Figure 8B). The molecular functions were similarly analyzed, and from Day 7 onwards, the functions involved in apoptosis, binding and transport are shown (Figure 8C). The analysis of pathways revealed that the pathways at different time points had their own characteristics, and some of them were reported to be related to melanoma (Table 5). For example, before the tumor can be observed, the RhoA signal was significantly enriched. RhoA is reported to be the main signal transduction factor activated by GPR56 in melanoma cells, thus promoting cell movement[75]. CMSP induces the differentiation of B16F1 melanoma cells through the RhoA-MARK signaling pathway[76]. The crosstalk between dendritic cells and natural killer cells may represent the mechanism by which growing tumors evade immune responses. This interaction has an important effect on the immune response of pathogens and potential tumor cells, as demonstrated in melanoma cells[77]. The FAK signal can inhibit the migration and metastasis of B16F10 cells, which may be a potential target for the treatment of melanoma[78]. Focal adhesion kinase (FAK) is a nonreceptor tyrosine kinase that is involved in tumor angiogenesis. In addition to its role as a kinase, FAK is involved in cell proliferation, adhesion, migration, invasion and apoptosis[79-82]; however, acute response signals, LXR/RXR activation, and FXR/RXR activation were significantly enriched after the tumor was observed. It has been reported that FXR/RXR activation may attempt to reduce

inflammation, usually in conjunction with LXR and other receptors, to activate homeostasis in cholesterol and triglyceride metabolism and inhibit inflammation[83].

A total of 86 homologous differential proteins were identified with the condition of "fold change > 1.5, p value < 0.05", among which 39 differential proteins were reported to be associated with melanoma (Table 6, Figure 9).

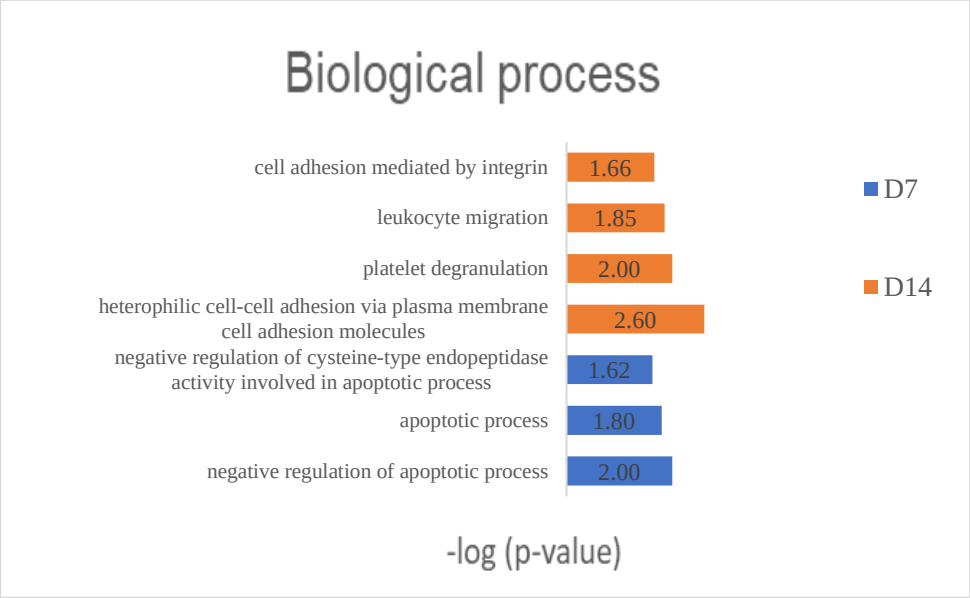

Figure 8A Biological process analysis of differential proteins in the B16 tumor-bearing mice

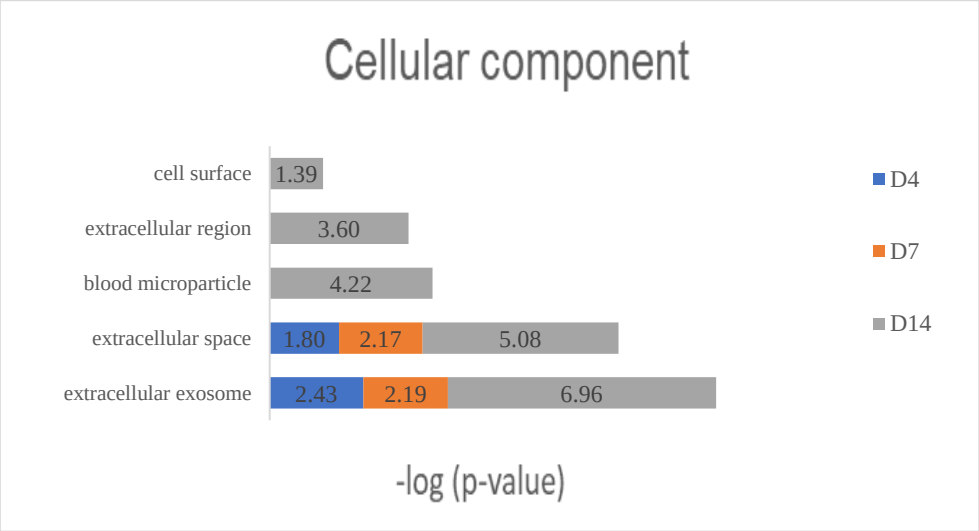

Figure 8B Cell component analysis of differential proteins in the B16 tumor-bearing mice

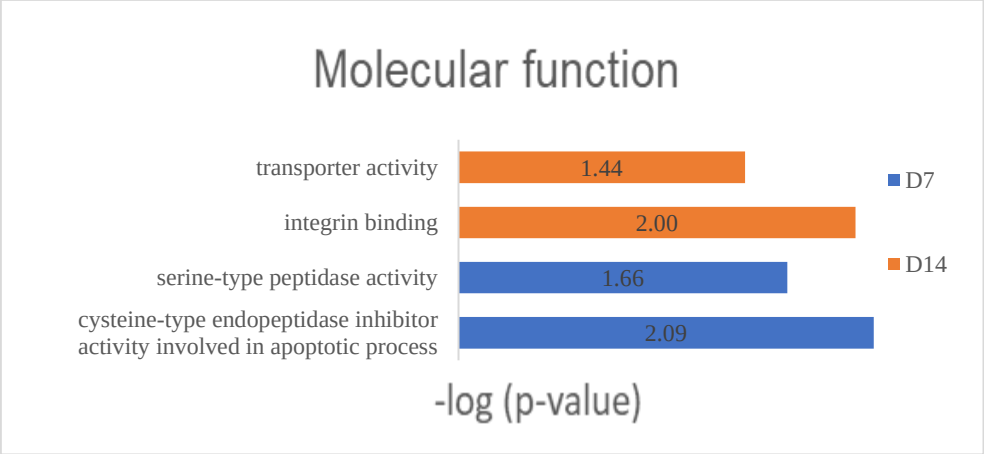

Figure 8C Molecular function analysis of differential proteins in the B16 tumor-bearing mice

Table 5 Pathway analysis of differential proteins in the B16 tumor-bearing mice

Term	-log(p-value)		
	D4	D7	D14
Glutaryl-CoA Degradation	2.5		
Tryptophan Degradation III (Eukaryotic)	2.35		
Mechanisms of Viral Exit from Host Cells	2.1	1.85	
Role of Oct4 in Mammalian Embryonic Stem Cell Pluripotency	2.05		
MSP-RON Signaling Pathway	1.94	1.7	
Remodeling of Epithelial Adherens Junctions	1.89	1.65	
Caveolar-mediated Endocytosis Signaling	1.84	1.61	
Agrin Interactions at Neuromuscular Junction	1.83	1.59	
VDR/RXR Activation	1.82		
Altered T Cell and B Cell Signaling in Rheumatoid Arthritis	1.79		
Regulation of Actin-based Motility by Rho	1.76	1.52	
Crosstalk between Dendritic Cells and Natural Killer Cells	1.76	1.52	
Death Receptor Signaling	1.75	1.51	
Fcγ Receptor-mediated Phagocytosis in Macrophages and Monocytes	1.74	1.5	
FAK Signaling	1.74	1.5	
VEGF Signaling	1.72	1.48	
Paxillin Signaling	1.68	1.44	
Virus Entry via Endocytic Pathways	1.68	1.44	
RhoA Signaling	1.63	1.39	
Cellular Effects of Sildenafil (Viagra)	1.61	1.37	
Epithelial Adherens Junction Signaling	1.53		

HOTAIR Regulatory Pathway	1.52	
Tec Kinase Signaling	1.51	
Germ Cell-Sertoli Cell Junction Signaling	1.49	
Tight Junction Signaling	1.49	
Agranulocyte Adhesion and Diapedesis	1.47	
RhoGDI Signaling	1.46	
Sertoli Cell-Sertoli Cell Junction Signaling	1.45	
ILK Signaling	1.44	
NRF2-mediated Oxidative Stress Response	1.44	
Clathrin-mediated Endocytosis Signaling	1.43	2.84
Leukocyte Extravasation Signaling	1.43	
Gap Junction Signaling	1.42	
Calcium Signaling	1.42	
Integrin Signaling	1.4	
Osteoarthritis Pathway	1.4	
EIF2 Signaling	1.39	
Actin Cytoskeleton Signaling	1.39	
Role of Osteoblasts, Osteoclasts and Chondrocytes in Rheumatoid Arthritis	1.38	
Signaling by Rho Family GTPases	1.33	
Acute Phase Response Signaling		5.74
Tumoricidal Function of Hepatic Natural Killer Cells		3.44
LXR/RXR Activation		3.42
Pentose Phosphate Pathway (Oxidative Branch)		2.33
Type I Diabetes Mellitus Signaling		2.15
Ceramide Degradation		2.15
Hepatic Fibrosis Signaling Pathway		2.07
Atherosclerosis Signaling		2.04
Sphingosine and Sphingosine-1-phosphate Metabolism		2.03
FXR/RXR Activation		2.02
IL-12 Signaling and Production in Macrophages		1.99
Prostanoid Biosynthesis		1.93
Pentose Phosphate Pathway		1.93
Granulocyte Adhesion and Diapedesis		1.8
Granzyme B Signaling		1.73

Extrinsic Prothrombin Activation Pathway	1.73
Parkinson's Signaling	1.73
Hepatic Fibrosis/Hepatic Stellate Cell Activation	1.71
Cytotoxic T Lymphocyte-mediated Apoptosis of Target Cells	1.42
TWEAK Signaling	1.4
Coagulation System	1.39
Complement System	1.38
Docosahexaenoic Acid (DHA) Signaling	1.36
Role of PKR in Interferon Induction and Antiviral Response	1.33
Intrinsic Prothrombin Activation Pathway	1.33
Role of Macrophages, Fibroblasts and Endothelial Cells in Rheumatoid Arthritis	1.32

Table 6A Differential proteins in the B16 tumor-bearing mice ($p<0.05$)

UniProt ID	Protein name	Fold change			PubMed
		D4	D7	D14	Melanoma
P39059	Collagen alpha-1(XV) chain	1.52			
P10451	Osteopontin	1.88	1.87	2.04	PMID: 28158294
P00915	Carbonic anhydrase 1	1.62			PMID: 30362384
Q9H3R2	Mucin-13	2.24		2.24	PMID: 29768245
Q06830	Peroxiredoxin-1				PMID: 19249851 PMID: 26285655 PMID: 28423711 PMID: 23749642
		0.62			PMID: 25627040
P60709	Actin, cytoplasmic 1	0.64	0.65		PMID: 23266771
P68032	Alpha-cardiac actin	0.42	0.46		PMID: 23266771
Q03403	Trefoil factor 2	1.58			
Q15113	Procollagen C-endopeptidase enhancer 1	1.53			
P35555	Fibrillin-1	0.61			PMID: 12807887
Q12841	Follistatin-related protein 1	1.53			
P43121	Cell surface glycoprotein MUC18	0.59			PMID: 9398060 PMID: 25729916
Q96PD5	N-acetylmuramoyl-L-alanine amidase	1.65			
Q9BTY2	Plasma alpha-L-fucosidase	0.65			

Q9NR71	Neutral ceramidase	1.67		2.08	PMID: 21700700
O75594	Peptidoglycan recognition protein 1		0.49		
O14773	Tripeptidyl-peptidase 1		0.65		PMID: 26365187
P40925	Malate dehydrogenase, cytoplasmic		0.66		
P30048	Peroxiredoxin-3		1.83		PMID: 25627040
P51674	Neuronal membrane glycoprotein M6-a		0.36		
P22692	Insulin-like growth factor-binding protein 4		0.49		PMID: 19025658
P08758	Annexin A5		0.54	0.43	PMID: 24743186 PMID: 28402934
P38606	V-type proton ATPase catalytic subunit A		1.74		
P31949	Protein S100-A11		0.61		
P06576	ATP synthase F1 subunit beta		0.44		PMID: 30537064
P55017	Solute carrier family 12 member 3		1.76	2.00	
P27348	14-3-3 protein theta		0.54		
Q8NC42	E3 ubiquitin-protein ligase RNF149		0.56		
P21796	Voltage-dependent anion-selective channel protein 1		1.68		PMID: 22539317
Q14393	Growth arrest-specific protein 6		1.51		
Q04756	Hepatocyte growth factor activator		0.66		PMID: 25910030
Q8N9V7	Protein TOPAZ1			1.86	
O00244	Copper transport protein ATOX1			2.42	PMID: 23988033
P41222	Prostaglandin-H2 D-isomerase			3.46	PMID: 25938039
P28039	Acyloxyacyl hydrolase			0.54	
Q8IV08	Phospholipase D3			0.57	PMID: 26118123
Q99519	Sialidase-1			0.52	
O95388	WNT1-inducible-signaling pathway protein 1			1.65	PMID: 30723155
P41217	OX-2 membrane glycoprotein			0.56	PMID: 18008004
P56537	Eukaryotic translation initiation factor 6			5.95	PMID: 28445515 PMID: 16850525
O75309	Cadherin-16			0.57	PMID: 29673969
P50897	Palmitoyl-protein thioesterase 1			0.58	
Q0KKI6	Immunoglobulin kappa constant			1.52	
P09603	Macrophage colony-stimulating factor 1			1.60	PMID: 28240048 PMID: 29643229
P04003	C4b-binding protein			2.64	

P0CG47	Polyubiquitin-B	1.61	
P06858	Lipoprotein lipase	0.57	PMID: 10628360
P05362	Intercellular adhesion molecule 1	0.56	PMID: 29245925
P00734	Prothrombin	1.73	PMID: 15567463
P02774	Vitamin D-binding protein	0.67	PMID: 1835629
P26038	Moesin	0.46	PMID: 19723803
P26927	Hepatocyte growth factor-like protein	1.93	
P28799	Progranulin	1.59	PMID: 31491449
Q92692	Nectin-2	1.99	
P55291	Cadherin-15	1.76	
P26842	CD27 antigen	0.45	
P61970	Nuclear transport factor 2	4.26	PMID: 26763446
P99999	Cytochrome c, somatic	3.14	
P68371	Tubulin beta-4B chain	0.47	
Q14515	SPARC-like protein 1	1.92	
P78310	CVB3-binding protein	1.64	
P17405	Acid sphingomyelinase	0.65	PMID: 25851537
			PMID: 30821848
		1.64	PMID: 30553852
Q08380	Galectin-3-binding protein		PMID: 26160844
Q9P1F3	Costars family protein ABRACL	4.46	
Q86UQ4	ATP-binding cassette sub-family A member 13	0.66	
P02763	Alpha-1-acid glycoprotein 1	0.66	
Q13443	Disintegrin and metalloproteinase domain-containing protein 9	2.20	PMID: 22622419 PMID: 21135106
Q9NPH3	Interleukin-1 receptor accessory protein	0.50	
P17813	Endoglin	1.64	PMID: 26712792
O14498	Immunoglobulin superfamily containing leucine-rich repeat protein	0.62	
Q99523	Sortilin	0.55	
Q8IXQ6	Protein mono-ADP-ribosyltransferase PARP9	5.05	
Q8NFZ8	Cell adhesion molecule 4	1.91	PMID: 11145252
Q9UJV8	Purine-rich element-binding protein gamma	0.24	
Q92520	Interleukin-like EMT inducer	2.01	PMID: 29871931

			PMID: 28545079
Q9BZP6	Acidic mammalian chitinase	0.51	
P02787	Transferrin	0.46	
O95336	6-phosphogluconolactonase	2.21	
Q9BRT3	Migration and invasion enhancer 1	5.14	
O43169	Cytochrome b5 type B	3.24	
Q6EMK4	Vasorin	0.32	
Q9NRX4	14 kDa phosphohistidine phosphatase	5.04	
O95571	Persulfide dioxygenase ETHE1, mitochondrial	2.03	
Q9UJA9	Ectonucleotide pyrophosphatase	0.66	PMID: 26190462 PMID: 29500864
A8MVZ5	Butyrophilin-like protein 10	1.79	
O95998	Interleukin-18-binding protein	0.65	PMID: 12543807

Table 6B Pathway analysis of differential proteins in the B16 tumor-bearing mice ($p<0.05$)

Term	-log(p-value)		
	D4	D7	D14
NRF2-mediated Oxidative Stress Response	3.5	1.89	
Mechanisms of Viral Exit from Host Cells	3.39	3.18	
MSP-RON Signaling Pathway	3.09	2.88	1.97
Remodeling of Epithelial Adherens Junctions	2.97	2.77	
Caveolar-mediated Endocytosis Signaling	2.89	2.68	
Agrin Interactions at Neuromuscular Junction	2.85	2.65	
Regulation of Actin-based Motility by Rho	2.73	2.52	
Crosstalk between Dendritic Cells and Natural Killer Cells	2.72	2.51	
Death Receptor Signaling	2.71	2.5	1.61
Fcγ Receptor-mediated Phagocytosis in Macrophages and Monocytes	2.68	2.47	
FAK Signaling	2.67	2.46	
VEGF Signaling	2.64	2.44	
Paxillin Signaling	2.57	2.36	
Virus Entry via Endocytic Pathways	2.56	2.35	
RhoA Signaling	2.46	2.25	
Cellular Effects of Sildenafil (Viagra)	2.42	2.22	
Ceramide Degradation	2.36		1.79

Epithelial Adherens Junction Signaling	2.27	2.07	
Sphingosine and Sphingosine-1-phosphate Metabolism	2.23		1.67
Tec Kinase Signaling	2.22	2.02	
Germ Cell-Sertoli Cell Junction Signaling	2.19	1.99	
Tight Junction Signaling	2.18	1.98	
Agranulocyte Adhesion and Diapedesis	2.14	1.94	
RhoGDI Signaling	2.13	1.93	1.91
Sertoli Cell-Sertoli Cell Junction Signaling	2.12	1.91	
ILK Signaling	2.1	1.9	
Clathrin-mediated Endocytosis Signaling	2.07	1.87	2.74
Leukocyte Extravasation Signaling	2.06	1.86	
Gap Junction Signaling	2.06	1.86	
Integrin Signaling	2.01	1.81	
EIF2 Signaling	1.98	1.79	
Actin Cytoskeleton Signaling	1.98	1.78	
Glutaryl-CoA Degradation	1.93		
Signaling by Rho Family GTPases	1.88	1.68	1.56
Tryptophan Degradation III (Eukaryotic)	1.77		
Role of Oct4 in Mammalian Embryonic Stem Cell Pluripotency	1.49	1.39	1.39
Mitochondrial Dysfunction		3.34	
IGF-1 Signaling		2.38	
Neuroprotective Role of THOP1 in Alzheimer's Disease		2.34	
Aspartate Degradation II		2.19	
Calcium Transport I		2.03	1.57
Osteoarthritis Pathway		1.8	2.63
TCA Cycle II (Eukaryotic)		1.65	
Gluconeogenesis I		1.64	
Sirtuin Signaling Pathway		1.55	1.55
Cell Cycle: G2/M DNA Damage Checkpoint Regulation		1.35	1.35
LXR/RXR Activation			4.73
Acute Phase Response Signaling			3.93
Atherosclerosis Signaling			3.47
FXR/RXR Activation			3.44
Tumoricidal Function of Hepatic Natural Killer Cells			2.72

UVA-Induced MAPK Signaling	2.64
Gα12/13 Signaling	2.28
CD27 Signaling in Lymphocytes	2.06
Granulocyte Adhesion and Diapedesis	2
Retinoic acid Mediated Apoptosis Signaling	1.98
Pentose Phosphate Pathway (Oxidative Branch)	1.97
Hepatic Fibrosis/Hepatic Stellate Cell Activation	1.88
Hepatic Fibrosis Signaling Pathway	1.79
Role of Osteoblasts, Osteoclasts and Chondrocytes in Rheumatoid Arthritis	1.69
Altered T Cell and B Cell Signaling in Rheumatoid Arthritis	1.67
Sphingomyelin Metabolism	1.67
Ceramide Signaling	1.63
Prostanoid Biosynthesis	1.57
Pentose Phosphate Pathway	1.57
Hematopoiesis from Multipotent Stem Cells	1.49
Acyl-CoA Hydrolysis	1.49
Type I Diabetes Mellitus Signaling	1.47
Choline Biosynthesis III	1.43
Sphingosine-1-phosphate Signaling	1.42
Role of Tissue Factor in Cancer	1.41
Granzyme B Signaling	1.37
Extrinsic Prothrombin Activation Pathway	1.37
Parkinson's Signaling	1.37
Role of Macrophages, Fibroblasts and Endothelial Cells in Rheumatoid Arthritis	1.32
IL-12 Signaling and Production in Macrophages	1.32

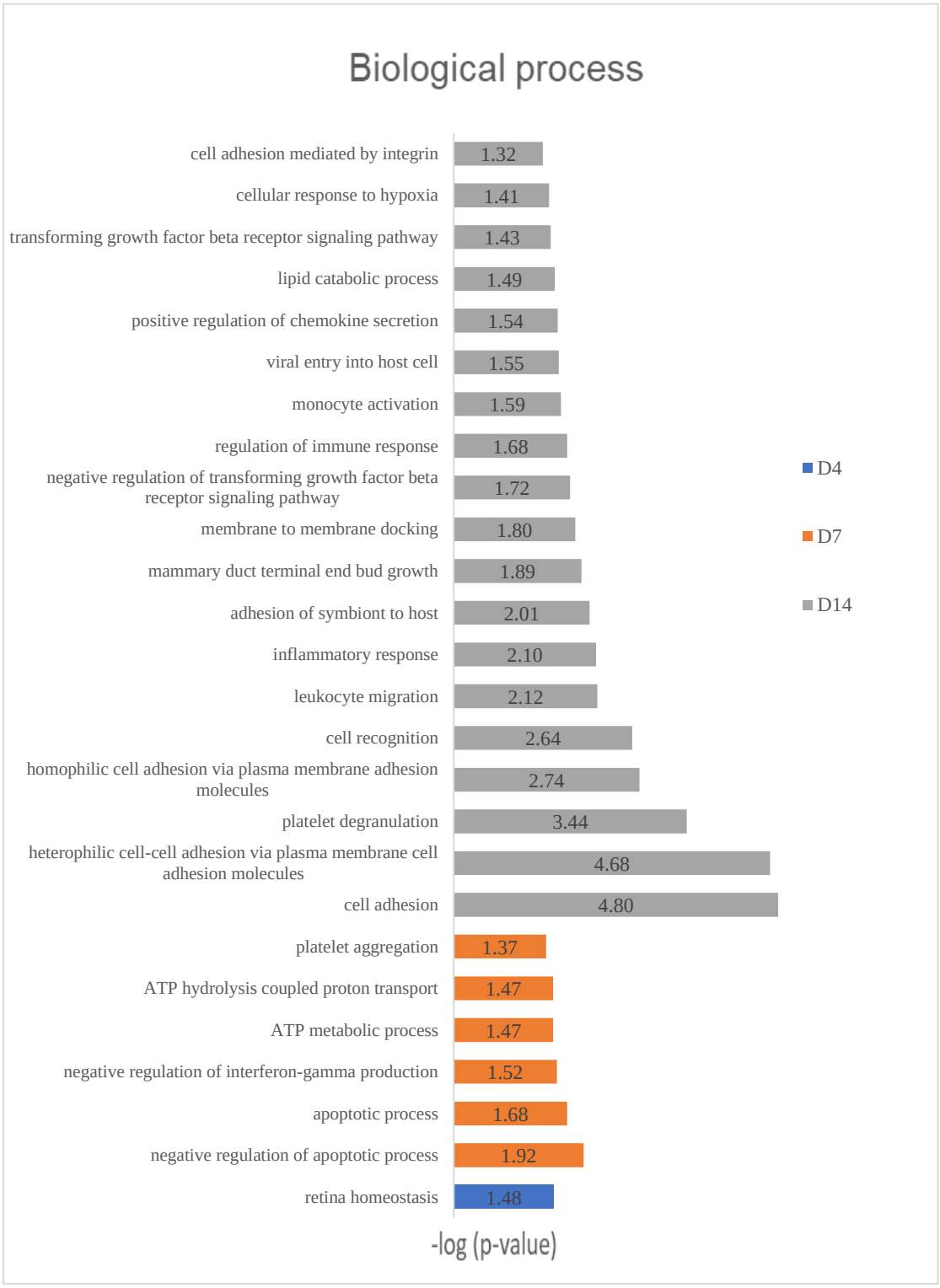

Figure 9A Biological process analysis of differential proteins in the B16 tumor-bearing mice ($p<0.05$)

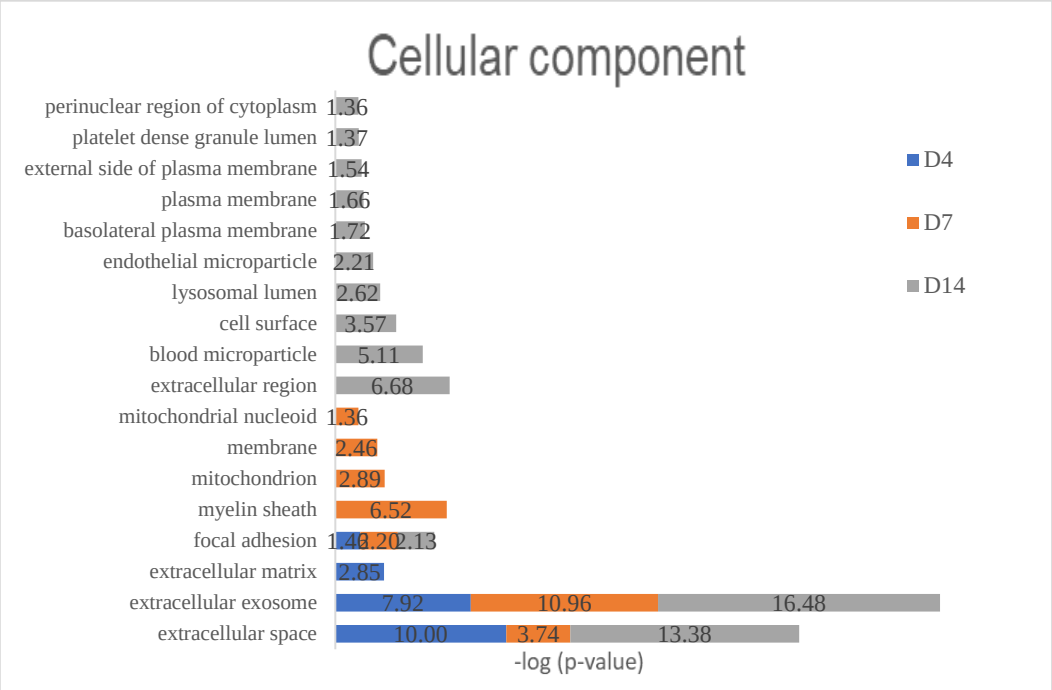

Figure 9B Cell component analysis of differential proteins in the B16 tumor-bearing mice ($p<0.05$)

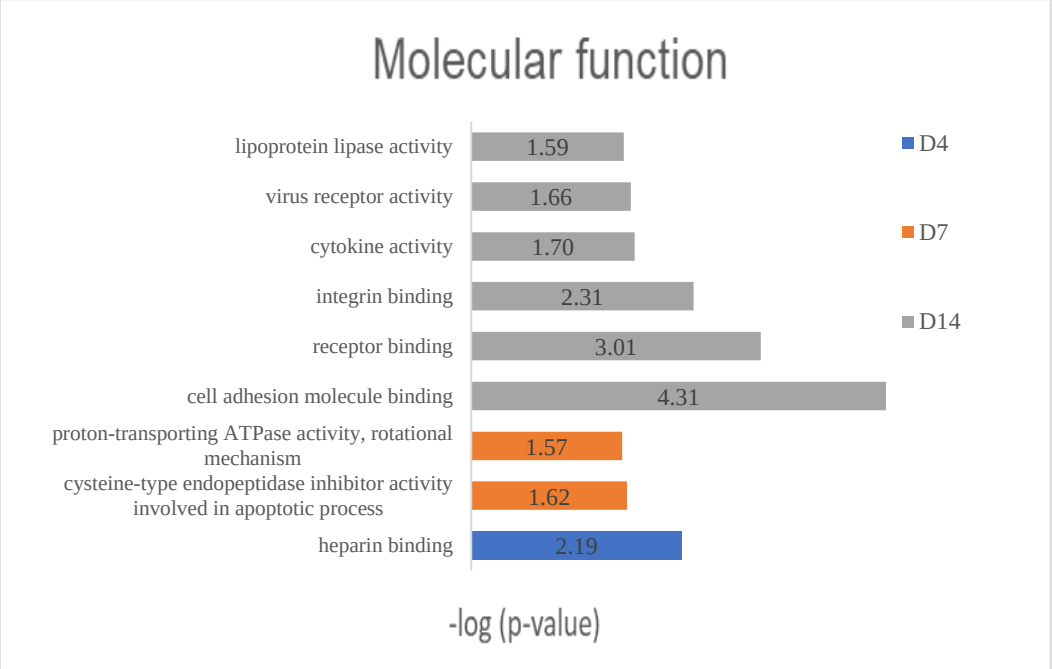

Figure 9C Molecular function analysis of differential proteins in the B16 tumor-bearing mice ($p<0.05$)

2.3.2 RM-1 prostate cancer-bearing mice

Analysis of biological processes showed metabolic and inflammatory processes on Day 7 and Day 22 and bone development on Day 15, suggesting that this process may be related to tumor bone

metastasis and is consistent with the trend of bone metastasis in prostate cancer (Figure 10A). Analysis of cell composition also revealed that the differential proteins were secreted proteins, mostly from the extracellular matrix and the cell surface (Figure 10B). Analysis of the molecular function revealed the activity of the channel protein (Figure 10C). Similarly, the pathway analysis showed that the pathways at different time points had their own characteristics, and some of them were reported to be associated with prostate cancer (Table 7). For example, before the tumor was palpable, FXR/RXR activation, LXR/RXR activation[83], mitochondrial dysfunction, acute phase response signaling and other pathways were significantly enriched. It has been reported that the activation of the LXR/RXR and FXR/RXR pathways may alleviate inflammation. RXR is a nuclear hormone receptor of the retinoid A receptor family, which is usually used with LXR and FXR receptors. These receptors usually exist in biological and pathological pathways related to glucose, lipid homeostasis and the inflammatory response[83]. The proteomic study of urine in prostate cancer patients with a Gleason score of 6.9 ± 1.1 showed that LXR/RXR is activated and the signal of the acute-phase response is significantly downregulated[84]. Clathrin-mediated endocytosis is associated with the migration of prostate cancer cells[85]. The regulation of Rho on actin movement is significantly enriched after the tumor is palpable. It has been reported that the RhoC gene can affect cell migration by regulating the actin cytoskeleton, thus affecting the invasion and metastasis of malignant tumors[86].

A total of 42 homologous differential proteins were identified with the condition of "fold change > 1.5, p value < 0.05", of which 23 were reported to be associated with prostate cancer (Table 8, Figure 11).

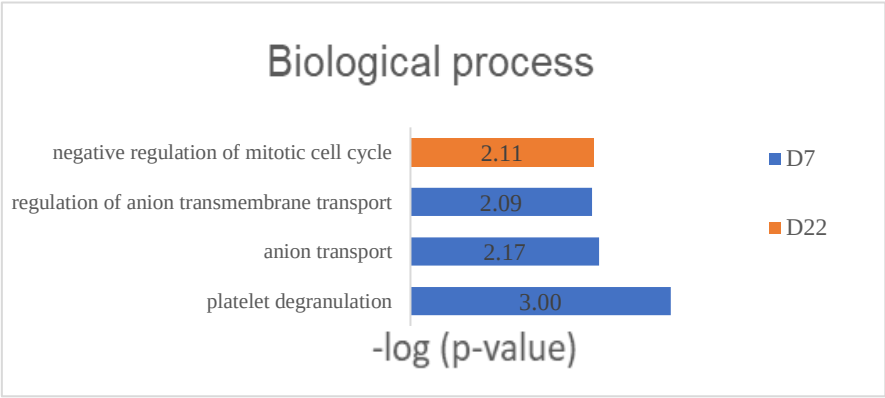

Figure 10A Biological process analysis of differential proteins in the RM-1 tumor-bearing mice

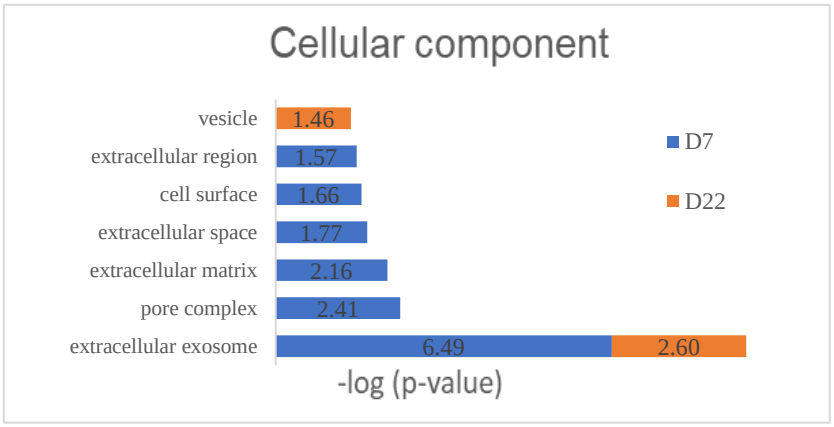

Figure 10B Cell component analysis of differential proteins in the RM-1 tumor-bearing mice

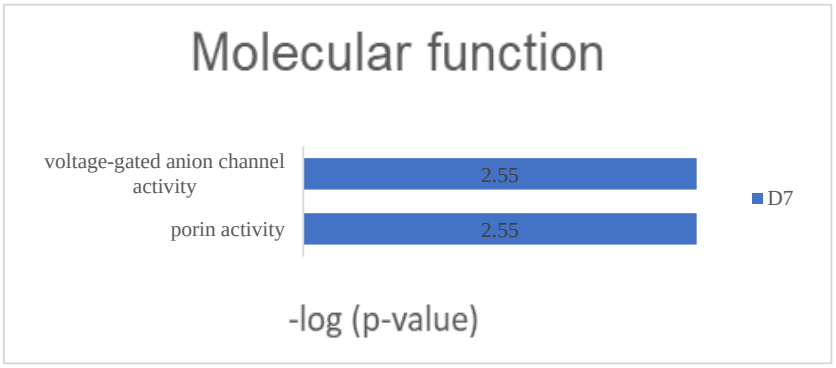

Figure 10C Biological process analysis of differential proteins in the RM-1 tumor-bearing mice

Table 7 Pathway analysis of differential proteins in the RM-1 tumor-bearing mice

Term	-log(p-value)	
	D7	D22
LXR/RXR Activation	4.77	1.45
FXR/RXR Activation	4.73	1.44
Atherosclerosis Signaling	2.9	
Mitochondrial Dysfunction	2.64	
Acute Phase Response Signaling	2.58	
Clathrin-mediated Endocytosis Signaling	2.52	
Sirtuin Signaling Pathway	2.19	
Glycogen Degradation III		2.42
Hepatic Fibrosis Signaling Pathway		2.35
Regulation of Actin-based Motility by Rho		1.59
PAK Signaling		1.55
Apelin Cardiomyocyte Signaling Pathway		1.54

CCR3 Signaling in Eosinophils	1.46
RhoA Signaling	1.45
Cellular Effects of Sildenafil (Viagra)	1.44
Cdc42 Signaling	1.43
Iron homeostasis signaling pathway	1.42
Tight Junction Signaling	1.32

Table 8A Differential proteins in the RM-1 tumor-bearing mice ($p<0.05$)

UniProt ID	Protein name	Fold change			PubMed
		D7	D15	D22	Prostate cancer
P98164	Low-density lipoprotein receptor-related protein 2	1.59			PMID: 28138564
Q16661	Guanylate cyclase activator 2B	0.25			
P12821	Angiotensin-converting enzyme	1.70			PMID: 29970692 PMID: 26760503
P07686	Beta-hexosaminidase subunit beta	1.80			PMID: 24389457
P01034	Cystatin-C	2.11			PMID: 28812020 PMID: 19956729 PMID: 16831167
Q14210	Lymphocyte antigen 6D	1.51			
P14091	Cathepsin E	1.56			PMID: 18006832 PMID: 20482316
O14745	Na(+)/H(+) exchange regulatory cofactor NHE-RF1	0.46		0.35	
Q9Y639	Neuroplastin	2.32			
P02749	Beta-2-glycoprotein 1	0.49			PMID: 24367699
Q02818	Nucleobindin-1	2.61			PMID: 30327690 PMID: 23958433
P17405	Acid sphingomyelinase	1.58			
P10909	Clusterin	1.51			PMID: 9815554 PMID: 26313417
Q9Y277	Voltage-dependent anion-selective channel protein 3 (VDAC-3) (mVDAC3) (Outer mitochondrial membrane protein porin 3)	1.70			PMID: 25177836
P21796	Voltage-dependent anion-selective channel protein	2.01			PMID: 30528266

	1				PMID: 25177836
Q15113	Procollagen C-endopeptidase enhancer 1	2.27		2.65	
Q92896	Golgi apparatus protein 1	1.62			
O14498	Immunoglobulin superfamily containing leucine-rich repeat protein	2.15			
P02787	Transferrin	0.64		0.58	PMID: 2433078 PMID: 7029542 PMID: 8989919 PMID: 28592703 PMID: 15619922 PMID: 29135121
P04066	Tissue alpha-L-fucosidase	1.69			
O60494	Cubilin	1.66			
P49747	Cartilage oligomeric matrix protein	0.52	0.56	0.54	PMID: 29228690 PMID: 31413818
O95497	Pantetheinase	1.69			
Q92485	Acid sphingomyelinase-like phosphodiesterase 3b		1.85		
Q92484	Acid sphingomyelinase-like phosphodiesterase 3a		1.75		
Q08380	Galectin-3-binding protein		1.70		PMID: 24205440
Q9Y653	Adhesion G-protein coupled receptor G1		1.53		
P04114	Apolipoprotein B-100			0.30	PMID: 21562751
P01833	Polymeric immunoglobulin receptor			1.55	
P07711	Cathepsin L1			1.79	PMID: 26757413
P00749	Urokinase-type plasminogen activator			1.62	PMID: 28278500
P09488	Glutathione S-transferase Mu 1			0.38	PMID: 27268642
P07195	L-lactate dehydrogenase B chain			0.47	PMID: 25983002
P28799	Progranulin			1.86	PMID: 25365768
P63104	14-3-3 protein zeta			2.01	
P10253	Lysosomal alpha-glucosidase			1.85	
P54826	Growth arrest-specific protein 1			1.81	PMID: 18974881 PMID: 1505026
Q9GZM5	Protein YIPF3			1.86	
Q15746	Myosin light chain kinase, smooth muscle			0.54	PMID: 29798970 PMID: 19429448

P59796	Glutathione peroxidase 6	2.39	
Q04756	Hepatocyte growth factor activator	2.11	PMID: 16005141 PMID: 29118397
O95998	Interleukin-18-binding protein	1.69	PMID: 20878981

Table 8B Pathway analysis of differential proteins in the RM-1 tumor-bearing mice ($p<0.05$)

Term	-log(p-value)		
	D7	D15	D22
LXR/RXR Activation	3.6		2.25
FXR/RXR Activation	3.56		2.22
Atherosclerosis Signaling	2.15		
Sphingomyelin Metabolism	2.08		
Mitochondrial Dysfunction	1.91		
Acute Phase Response Signaling	1.84		
Chondroitin Sulfate Degradation (Metazoa)	1.84		
Dermatan Sulfate Degradation (Metazoa)	1.81		
Clathrin-mediated Endocytosis Signaling	1.78		1.87
Sirtuin Signaling Pathway	1.47		
tRNA Splicing		4.36	
Cardiac β-adrenergic Signaling		3.33	
Relaxin Signaling		3.29	
Gustation Pathway		3.27	
cAMP-mediated signaling		2.92	
G-Protein Coupled Receptor Signaling		2.77	
Protein Kinase A Signaling		2.47	1.31
Cardiac Hypertrophy Signaling (Enhanced)		2.28	
Glutathione Redox Reactions I			3.72
Apelin Adipocyte Signaling Pathway			2.61
Pyruvate Fermentation to Lactate			2.33
Glycogen Degradation III			1.92
Glutathione-mediated Detoxification			1.64
Coagulation System			1.49
Oncostatin M Signaling			1.4
Hepatic Fibrosis Signaling Pathway			1.36

Cell Cycle: G2/M DNA Damage Checkpoint	
Regulation	1.35
Autophagy	1.32

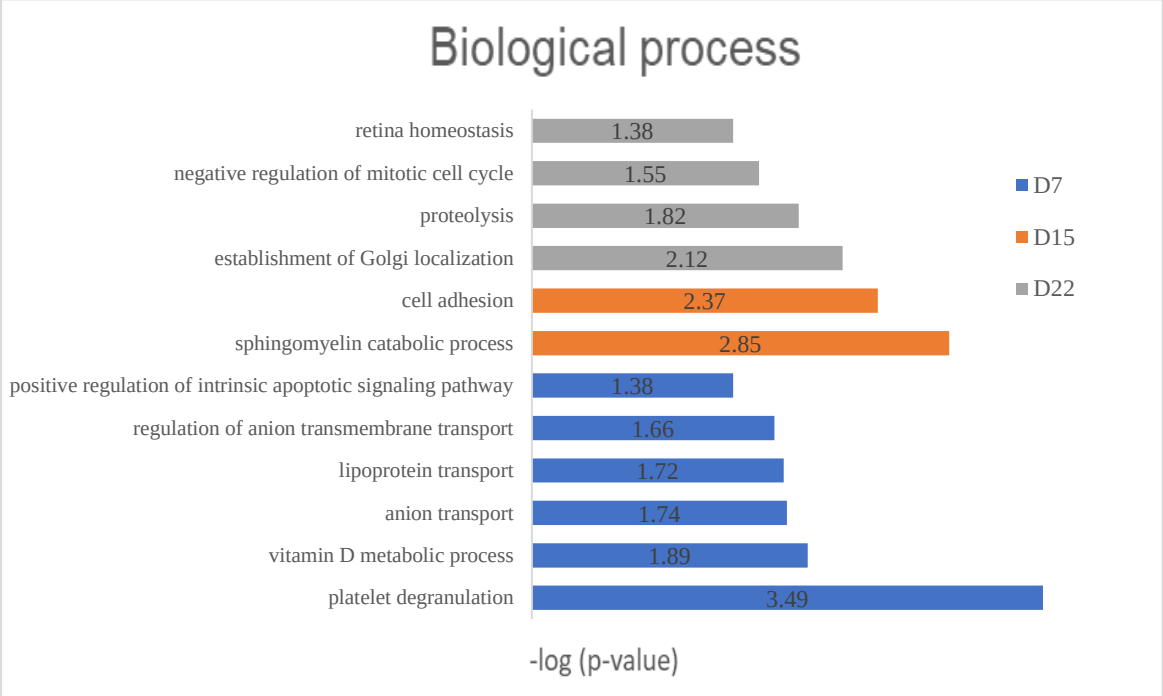

Figure 11A Biological process analysis of differential proteins in the RM-1 tumor-bearing mice ($p<0.05$)

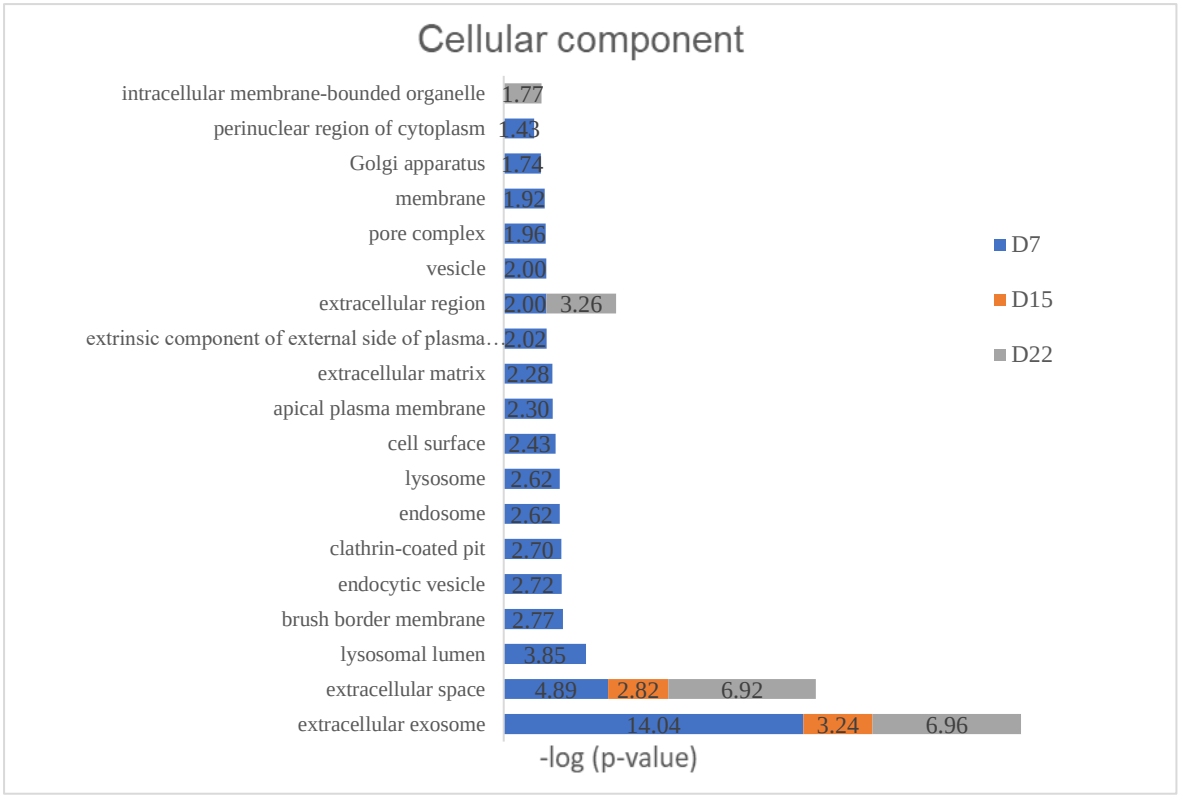

Figure 11B Cell component analysis of differential proteins in the RM-1 tumor-bearing mice ($p<0.05$)

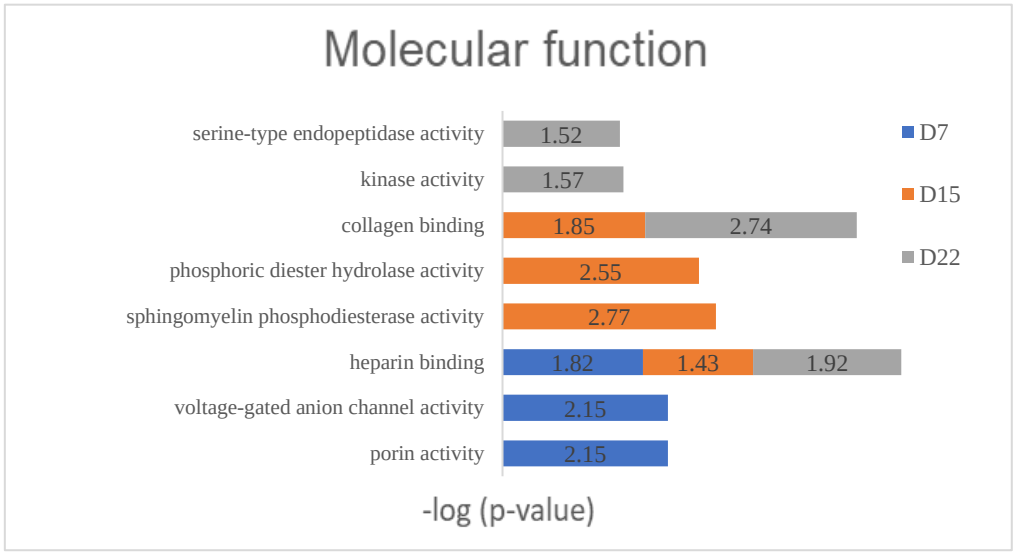

Figure 11C Molecular function analysis of differential proteins in the RM-1 tumor-bearing mice ($p<0.05$)

3 Conclusion

Random group analysis of samples can independently select better screening conditions according to the specific situation of experimental data, which is conducive to finding a group of differential proteins with higher reliability, and combination or linkage of differential proteins can further improve the reliability of markers. Furthermore, the reliability of differential proteins is related to the development of disease and the number of animals. To maximize the reliability of urine proteome changes, researchers can increase the number of experimental animals in future studies of urine biomarkers, particularly for early studies of diseases or diseases with little variation.

The results of this study showed that the urine proteome could reflect changes in the development of melanoma and prostate cancer cells. Before the tumor was detectable, significantly differential proteins were identified in the urine of both the B16 melanoma and RM-1 prostate tumor-bearing models. Moreover, there are major differences among the tumor-bearing models, suggesting that urine has good potential for early diagnosis, differentiation of different tumor types and development. Eventually, the different combinations of biomarkers can provide new ideas and clues for the early diagnosis of a tumor, which has the value in large-scale clinical research.

References:

1. Ferlay, J., et al., *Cancer incidence and mortality worldwide: Sources, methods and major patterns in GLOBOCAN 2012.* International Journal of Cancer, 2015. **136**(5): p. E359-E386.
2. Li, H., et al., *Primary malignant melanoma of the duodenum without visible melanin pigment: a mimicker of lymphoma or carcinoma.* Diagn Pathol, 2012. **7**: p. 74.
3. Hugo, W., et al., *Genomic and Transcriptomic Features of Response to Anti-PD-1 Therapy in Metastatic Melanoma.* Cell, 2016. **165**(1): p. 35-44.
4. Caenepeel, S., et al., *MAPK pathway inhibition induces MET and GAB1 levels, priming BRAF mutant melanoma for rescue by hepatocyte growth factor.* Oncotarget, 2017. **8**(11): p. 17795-17809.
5. Hamid, O., et al., *Five-year survival outcomes for patients with advanced melanoma treated with pembrolizumab in KEYNOTE-001.* Ann Oncol, 2019. **30**(4): p. 582-588.
6. Aubuchon, M.M.F., et al., *Epidemiology, management and survival outcomes of primary cutaneous melanoma: a ten-year overview.* Acta Chirurgica Belgica: p. 1-7.

7. Siegel, R.L., K.D. Miller, and A. Jemal, *Cancer statistics, 2018.* CA: A Cancer Journal for Clinicians, 2018. **68**(1): p. 7-30.
8. Ito, K., *Prostate cancer in Asian men.* Nature Reviews Urology, 2014. **11**: p. 197.
9. Cary, K.C. and M.R. Cooperberg, *Biomarkers in prostate cancer surveillance and screening: past, present, and future.* Ther Adv Urol, 2013. **5**(6): p. 318-29.
10. Wu, D., et al., *Urinary biomarkers in prostate cancer detection and monitoring progression.* Critical Reviews in Oncology/Hematology, 2017. **118**: p. 15-26.
11. Obirieze, A.C., et al., *African-American Men with Low-Risk Prostate Cancer: Modern Treatment and Outcome Trends.* Journal of Racial and Ethnic Health Disparities, 2015. **2**(3): p. 295-302.
12. Strimbu, K. and J.A. Tavel, *What are biomarkers?* Curr Opin HIV AIDS, 2010. **5**(6): p. 463-6.
13. Gerszten, R.E. and T.J. Wang, *The search for new cardiovascular biomarkers.* Nature, 2008. **451**(7181): p. 949-952.
14. Gao, Y., *Urine—an untapped goldmine for biomarker discovery?* Science China Life Sciences, 2013. **56**(12): p. 1145-1146.
15. Wu, J. and Y. Gao, *Physiological conditions can be reflected in human urine proteome and metabolome.* Expert Review of Proteomics, 2015. **12**(6): p. 623-636.
16. Wu, J., Z. Guo, and Y. Gao, *Dynamic changes of urine proteome in a Walker 256 tumor-bearing rat model.* Cancer medicine, 2017. **6**(11): p. 2713-2722.
17. Zhang, L., Y. Li, and Y. Gao, *Early changes in the urine proteome in a diethyldithiocarbamate-induced chronic pancreatitis rat model.* Journal of Proteomics, 2018. **186**: p. 8-14.
18. Kormosh, N.G., et al., *Conformational changes in inter-alpha-trypsin inhibitor heavy chain 4 activate its tumor-specific activity in mice with B16 melanoma.* 2015. **12**(3): p. 4483.
19. Wu, C.-M., X.-Y. Li, and T.-H. Huang, *Anti-tumor effect of pEgr-IFNgamma gene-radiotherapy in B16 melanoma-bearing mice.* World journal of gastroenterology, 2004. **10**(20): p. 3011-3015.
20. Xiong, F., Y.-Z. Mou, and X.-Y. Xiang, *Inhibition of mouse B16 melanoma by sodium butyrate correlated to tumor associated macrophages differentiation suppression.* International journal of clinical and experimental medicine, 2015. **8**(3): p. 4170-4174.
21. Ming, M., et al., *Therapeutic effect of oridonin on mice with prostate cancer.* Asian Pacific Journal of Tropical Medicine, 2016. **9**(2): p. 184-187.
22. Wei, S.-M., et al., *Anti-CD27 Antibody Potentiates Antitumor Effect of Dendritic Cell-Based Vaccine in Prostate Cancer-Bearing Mice.* International surgery, 2015. **100**(1): p. 155-163.
23. Wiśniewski, J.R., et al., *Universal sample preparation method for proteome analysis.* Nature Methods, 2009. **6**(5): p. 359-362.
24. Konstantakou, E.G., et al., *Deep-proteome mapping of WM-266-4 human metastatic melanoma cells: From oncogenic addiction to druggable targets.*

PLoS One, 2017. **12**(2): p. e0171512.

25. Rangaswami, H., A. Bulbule, and G.C. Kundu, *Osteopontin: role in cell signaling and cancer progression.* Trends Cell Biol, 2006. **16**(2): p. 79-87.
26. Andreucci, E., et al., *The carbonic anhydrase IX inhibitor SLC-0111 sensitises cancer cells to conventional chemotherapy.* Journal of enzyme inhibition and medicinal chemistry, 2019. **34**(1): p. 117-123.
27. Filippou, P.S., et al., *Exploring the potential of mucin 13 (MUC13) as a biomarker for carcinomas and other diseases.* Clin Chem Lab Med, 2018. **56**(11): p. 1945-1953.
28. Butcher, D.T., T. Alliston, and V.M. Weaver, *A tense situation: forcing tumour progression.* Nat Rev Cancer, 2009. **9**(2): p. 108-22.
29. Paszek, M.J., et al., *Tensional homeostasis and the malignant phenotype.* Cancer Cell, 2005. **8**(3): p. 241-54.
30. Guo, C., et al., *ACTB in cancer.* Clin Chim Acta, 2013. **417**: p. 39-44.
31. Hwang, S., et al., *Epigenetic Silencing of SPINT2 Promotes Cancer Cell Motility via HGF-MET Pathway Activation in Melanoma.* The Journal of investigative dermatology, 2015. **135**(9): p. 2283-2291.
32. Yu, J.Z., et al., *Assessing the clinical utility of measuring Insulin-like Growth Factor Binding Proteins in tissues and sera of melanoma patients.* J Transl Med, 2008. **6**: p. 70.
33. Hintsala, H.R., et al., *Dysregulation of redox-state-regulating enzymes in melanocytic skin tumours and the surrounding microenvironment.* Histopathology, 2015. **67**(3): p. 348-57.
34. Liu, J., et al., *Dissecting Fission Yeast Shelterin Interactions via MICro-MS Links Disruption of Shelterin Bridge to Tumorigenesis.* Cell Rep, 2015. **12**(12): p. 2169-80.
35. Palm-Espling, M.E., et al., *Interaction between the anticancer drug Cisplatin and the copper chaperone Atox1 in human melanoma cells.* Protein Pept Lett, 2014. **21**(1): p. 63-8.
36. Nyakas, M., et al., *Prognostic biomarkers for immunotherapy with ipilimumab in metastatic melanoma.* Clinical and experimental immunology, 2019. **197**(1): p. 74-82.
37. Morandi, F., et al., *Serum levels of cytoplasmic melanoma-associated antigen at diagnosis may predict clinical relapse in neuroblastoma patients.* Cancer immunology, immunotherapy : CII, 2011. **60**(10): p. 1485-1495.
38. Giansanti, F., et al., *Secreted Gal-3BP is a novel promising target for non-internalizing Antibody–Drug Conjugates.* Journal of Controlled Release, 2019. **294**: p. 176-184.
39. Duckworth, C.A., et al., *Chemically modified, non-anticoagulant heparin derivatives are potent galectin-3 binding inhibitors and inhibit circulating galectin-3-promoted metastasis.* Oncotarget, 2015. **6**(27): p. 23671-23687.
40. Kirszberg, C., V.M. Rumjanek, and R.Q. Monteiro, *Assembly and regulation of prothrombinase complex on B16F10 melanoma cells.* Thrombosis Research, 2005. **115**(1): p. 123-129.

41. Shi, K., et al., *Identify the signature genes for diagnose of uveal melanoma by weight gene co-expression network analysis.* International journal of ophthalmology, 2015. **8**(2): p. 269-274.
42. Galore-Haskel, G., et al., *Histopathological expression analysis of intercellular adhesion molecule 1 (ICAM-1) along development and progression of human melanoma.* Oncotarget, 2017. **8**(59): p. 99580-99586.
43. Fukami, T., et al., *Isolation of the mouse Tsll1 and Tsll2 genes, orthologues of the human TSLC1-like genes 1 and 2 (TSLL1 and TSLL2).* Gene, 2003. **323**: p. 11-8.
44. Koch, M.B., et al., *Microphthalmia Transcription Factor and Melanoma Cell Adhesion Molecule Expression Distinguish Desmoplastic/Spindle Cell Melanoma From Morphologic Mimics.* American Journal of Surgical Pathology. **25**(1): p. 58-64.
45. Pathria, G., et al., *RanBP3 Regulates Melanoma Cell Proliferation via Selective Control of Nuclear Export.* Journal of Investigative Dermatology, 2016. **136**(1): p. 264-274.
46. Miluzio, A., et al., *Impairment of cytoplasmic eIF6 activity restricts lymphomagenesis and tumor progression without affecting normal growth.* Cancer Cell, 2011. **19**(6): p. 765-75.
47. Welinder, C., et al., *Correlation of histopathologic characteristics to protein expression and function in malignant melanoma.* PLOS ONE, 2017. **12**(4): p. e0176167.
48. Guaiquil, V., et al., *ADAM9 is involved in pathological retinal neovascularization.* Mol Cell Biol, 2009. **29**(10): p. 2694-703.
49. Abety, A.N., et al., *Stromal fibroblast-specific expression of ADAM-9 modulates proliferation and apoptosis in melanoma cells in vitro and in vivo.* J Invest Dermatol, 2012. **132**(10): p. 2451-2458.
50. Zigrino, P., R. Nischt, and C. Mauch, *The disintegrin-like and cysteine-rich domains of ADAM-9 mediate interactions between melanoma cells and fibroblasts.* J Biol Chem, 2011. **286**(8): p. 6801-7.
51. Bedia, C., et al., *Acid ceramidase expression modulates the sensitivity of A375 melanoma cells to dacarbazine.* J Biol Chem, 2011. **286**(32): p. 28200-9.
52. Muhammad, L.A. and F. Saad, *The role of clusterin in prostate cancer: treatment resistance and potential as a therapeutic target.* 2015. **15**(9): p. 1049.
53. Steinberg, J., et al., *Intracellular levels of SGP-2 (Clusterin) correlate with tumor grade in prostate cancer.* Clinical Cancer Research, 1997. **3**(10): p. 1707-1711.
54. Kaighn, M.E., et al., *Growth control of prostatic carcinoma cells in serum-free media: interrelationship of hormone response, cell density, and nutrient media.* Proc Natl Acad Sci U S A, 1981. **78**(9): p. 5673-6.
55. Rossi, M.C. and B.R. Zetter, *Selective stimulation of prostatic carcinoma cell proliferation by transferrin.* Proc Natl Acad Sci U S A, 1992. **89**(13): p. 6197-201.
56. Bhatti, R.A., J.J. Gadarowski, and P.S. Ray, *Metastatic behavior of prostatic*

tumor as influenced by the hematopoietic and hematogenous factors. Tumour Biol, 1997. **18**(1): p. 1-5.

57. Aggarwal, R., et al., *Real-Time Transferrin-Based PET Detects MYC-Positive Prostate Cancer.* Mol Cancer Res, 2017. **15**(9): p. 1221-1229.
58. Grayhack, J.T., et al., *Biochemical profiles of prostatic fluid from normal and diseased prostate glands.* Prostate, 1980. **1**(2): p. 227-37.
59. Fernandez, C., et al., *A preliminary study of urinary transferrin as a marker for prostatic cancer.* Clin Chim Acta, 1986. **161**(3): p. 335-9.
60. Asmarinah, A., et al., *Expression of the Bcl-2 family genes and complexes involved in the mitochondrial transport in prostate cancer cells.* Int J Oncol, 2014. **45**(4): p. 1489-96.
61. Xue, Y.N., et al., *Zinc and p53 disrupt mitochondrial binding of HK2 by phosphorylating VDAC1.* Exp Cell Res, 2019. **374**(1): p. 249-258.
62. Englund, E., et al., *Cartilage oligomeric matrix protein promotes prostate cancer progression by enhancing invasion and disrupting intracellular calcium homeostasis.* Oncotarget, 2017. **8**(58): p. 98298-98311.
63. Rosas, S., et al., *Cartilage oligomeric matrix protein in patients with osteoarthritis is independently associated with metastatic disease in prostate cancer.* Oncotarget, 2019. **10**(46): p. 4776-4785.
64. DiNatale, A. and A. Fatatis, *The Bone Microenvironment in Prostate Cancer Metastasis.* Adv Exp Med Biol, 2019. **1210**: p. 171-184.
65. Stafford, J.H., et al., *Highly specific PET imaging of prostate tumors in mice with an iodine-124-labeled antibody fragment that targets phosphatidylserine.* PLoS One, 2013. **8**(12): p. e84864.
66. Yin, F., et al., *Exaggerated inflammation, impaired host defense, and neuropathology in progranulin-deficient mice.* J Exp Med, 2010. **207**(1): p. 117-28.
67. He, Z., et al., *Progranulin is a mediator of the wound response.* Nat Med, 2003. **9**(2): p. 225-9.
68. Tanimoto, R., et al., *Sortilin regulates progranulin action in castration-resistant prostate cancer cells.* Endocrinology, 2015. **156**(1): p. 58-70.
69. Del Sal, G., et al., *The growth arrest-specific gene, gas1, is involved in growth suppression.* Cell, 1992. **70**(4): p. 595-607.
70. Rizzi, F., et al., *A novel gene signature for molecular diagnosis of human prostate cancer by RT-qPCR.* PLoS One, 2008. **3**(10): p. e3617.
71. Leveille, N., A. Fournier, and C. Labrie, *Androgens down-regulate myosin light chain kinase in human prostate cancer cells.* J Steroid Biochem Mol Biol, 2009. **114**(3-5): p. 174-9.
72. Dai, Y., et al., *Circular RNA Myosin Light Chain Kinase (MYLK) Promotes Prostate Cancer Progression through Modulating Mir-29a Expression.* Med Sci Monit, 2018. **24**: p. 3462-3471.
73. Yhee, J.Y., et al., *Tumor-Targeting Transferrin Nanoparticles for Systemic Polymerized siRNA Delivery in Tumor-Bearing Mice.* Bioconjugate Chemistry, 2013. **24**(11): p. 1850-1860.

74. Kawamoto, M., et al., *Immunogenicity and toxicity of transferrin receptor-targeted hybrid peptide as a potent anticancer agent.* Cancer Chemotherapy and Pharmacology, 2013. **71**(3): p. 799-807.
75. Chiang, N.-Y., et al., *GPR56/ADGRG1 Activation Promotes Melanoma Cell Migration via NTF Dissociation and CTF-Mediated Gα12/13/RhoA Signaling.* Journal of Investigative Dermatology, 2017. **137**(3): p. 727-736.
76. Zhao, L., et al., *P-Hydroxycinnamaldehyde Induces B16-F1 Melanoma Cell Differentiation via the RhoA-MAPK Signaling Pathway.* Cellular Physiology and Biochemistry, 2016. **38**(6): p. 2247-2260.
77. Capobianco, A., et al., *Melanoma cells interfere with the interaction of dendritic cells with NK/LAK cells.* Int J Cancer, 2006. **119**(12): p. 2861-9.
78. Pei, G., et al., *FAK regulates E-cadherin expression via p-SrcY416/p-ERK1/2/p-Stat3Y705 and PPARgamma/miR-125b/Stat3 signaling pathway in B16F10 melanoma cells.* Oncotarget, 2017. **8**(8): p. 13898-13908.
79. Luo, M. and J.L. Guan, *Focal adhesion kinase: a prominent determinant in breast cancer initiation, progression and metastasis.* Cancer Lett, 2010. **289**(2): p. 127-39.
80. Arold, S.T., *How focal adhesion kinase achieves regulation by linking ligand binding, localization and action.* Curr Opin Struct Biol, 2011. **21**(6): p. 808-13.
81. Sulzmaier, F.J., C. Jean, and D.D. Schlaepfer, *FAK in cancer: mechanistic findings and clinical applications.* Nat Rev Cancer, 2014. **14**(9): p. 598-610.
82. Tavora, B., et al., *Endothelial FAK is required for tumour angiogenesis.* EMBO Mol Med, 2010. **2**(12): p. 516-28.
83. Kong, Z., et al., *Multi-Omics Analysis Reveals Up-Regulation of APR Signaling, LXR/RXR and FXR/RXR Activation Pathways in Holstein Dairy Cows Exposed to High-Altitude Hypoxia.* Animals : an open access journal from MDPI, 2019. **9**(7): p. 406.
84. Davalieva, K., et al., *Comparative Proteomics Analysis of Urine Reveals Down-Regulation of Acute Phase Response Signaling and LXR/RXR Activation Pathways in Prostate Cancer.* Proteomes, 2017. **6**(1): p. 1.
85. Satcher, R.L., et al., *Cadherin-11 endocytosis through binding to clathrin promotes cadherin-11-mediated migration in prostate cancer cells.* J Cell Sci, 2015. **128**(24): p. 4629-41.
86. Yuan, Z., et al., *[Correlation of expression of RhoC with invasiveness of prostate cancer cell line PC-3M in vitro].* Zhonghua Yi Xue Za Zhi, 2008. **88**(1): p. 51-5.

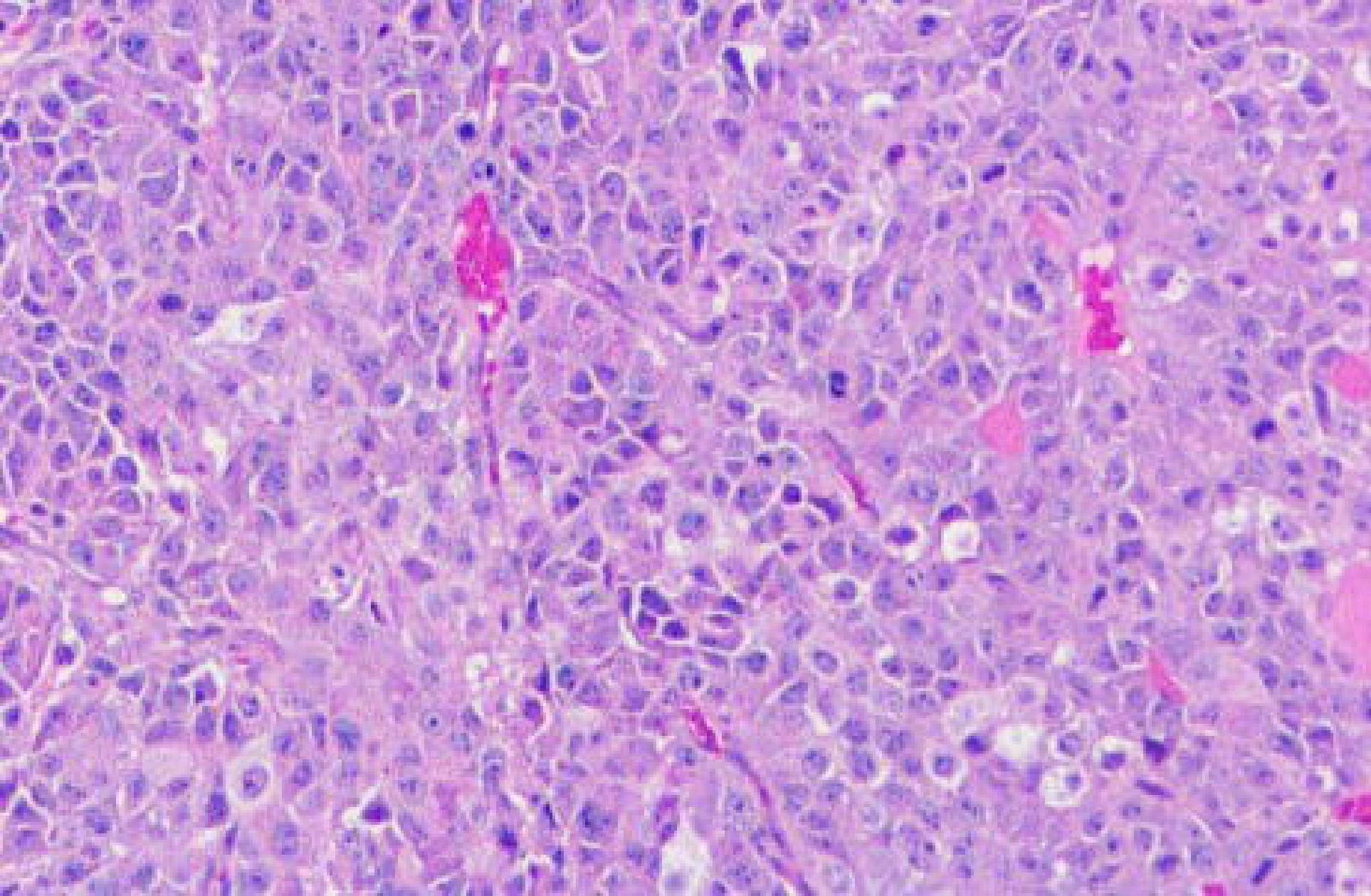

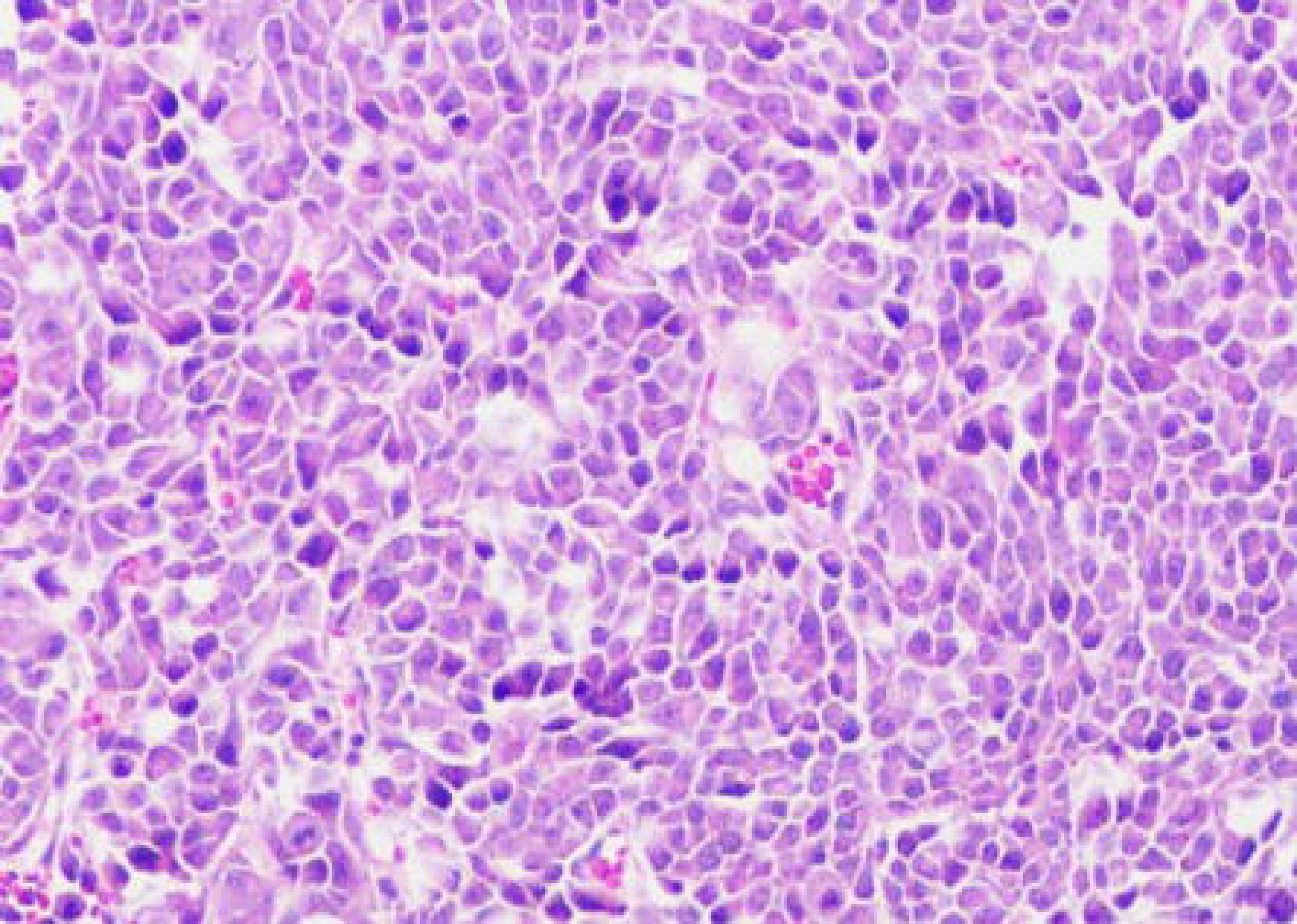

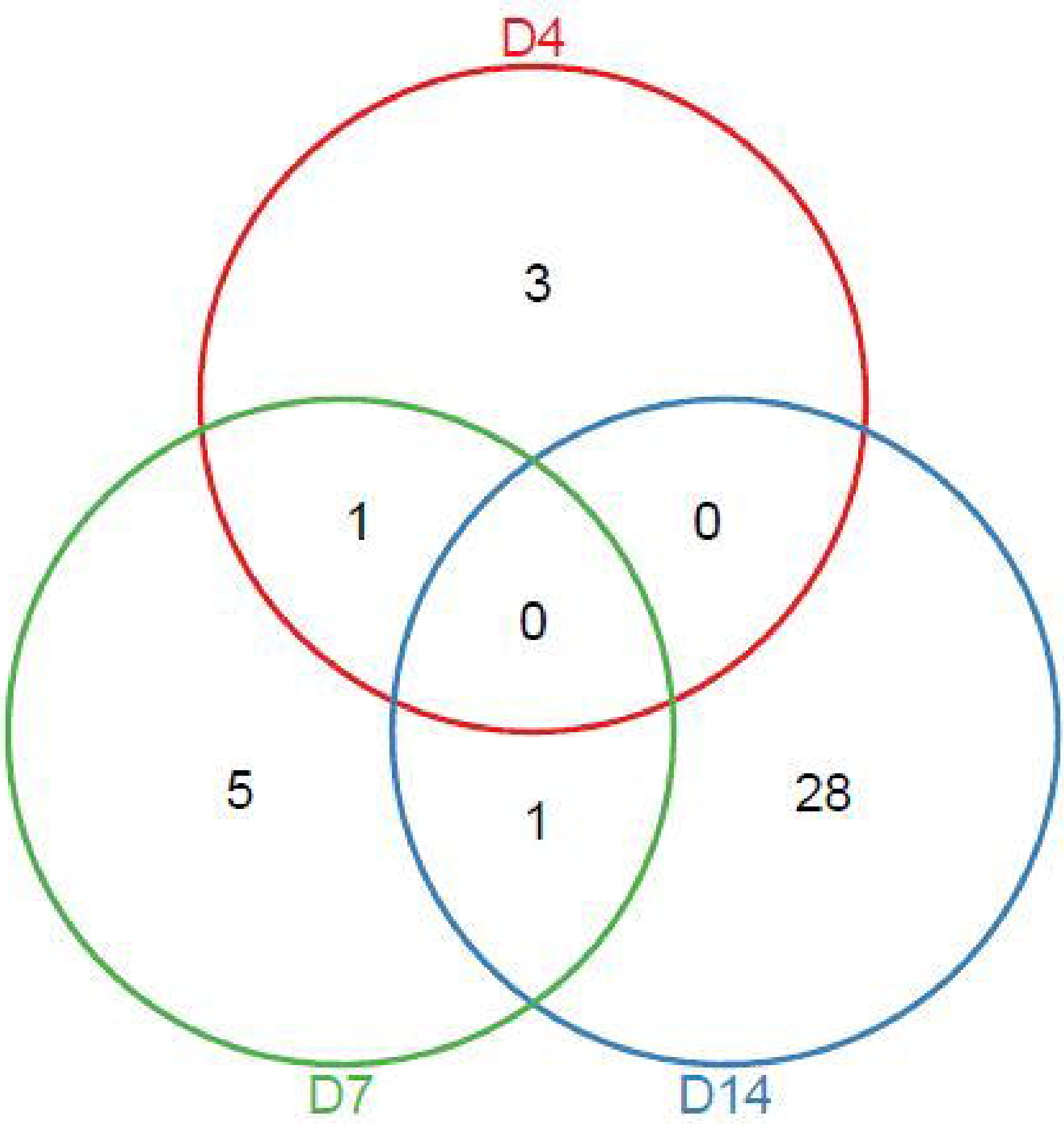
D4
3
1
0
0
5
1
28
D7
D14

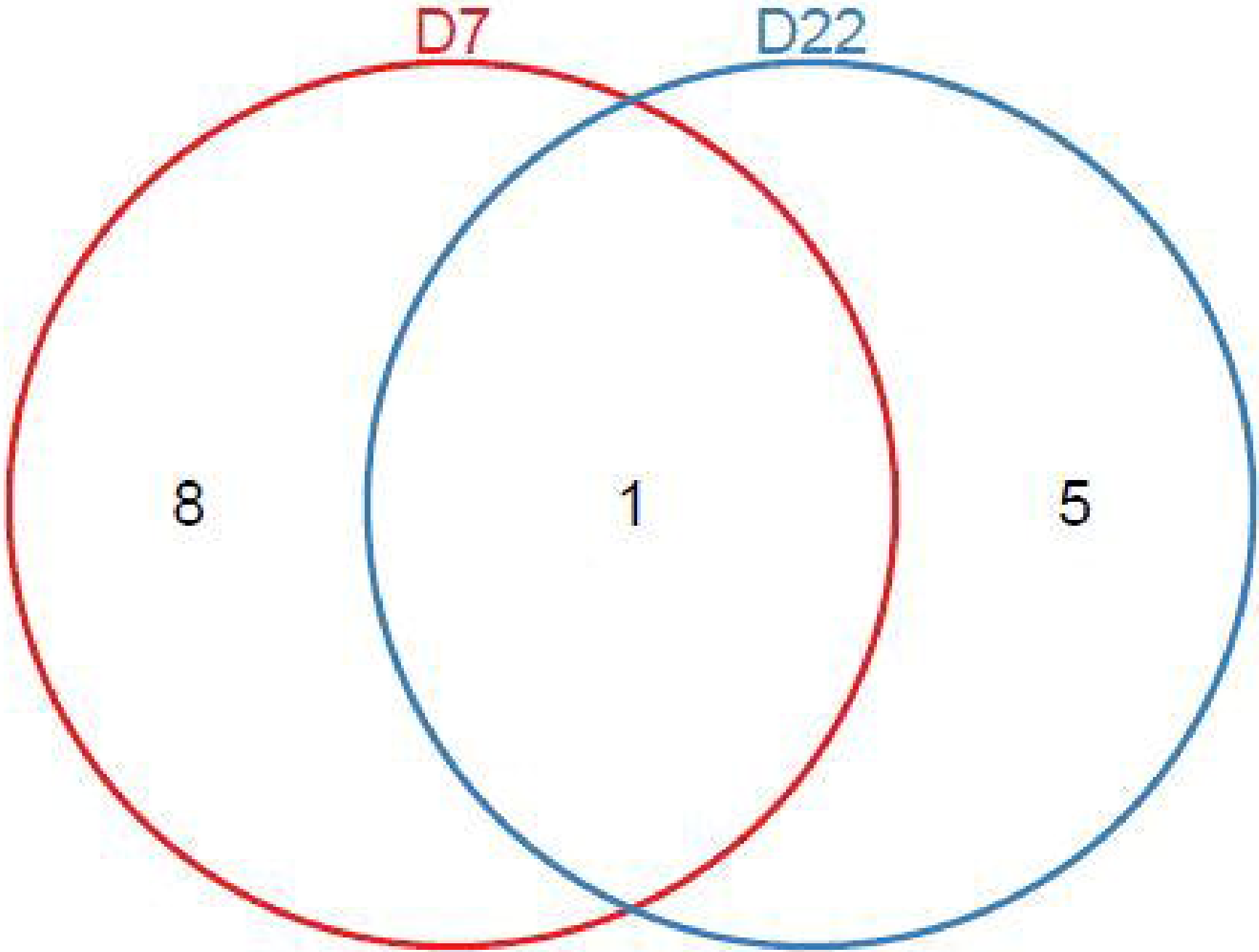
D7
D22
8
1
5

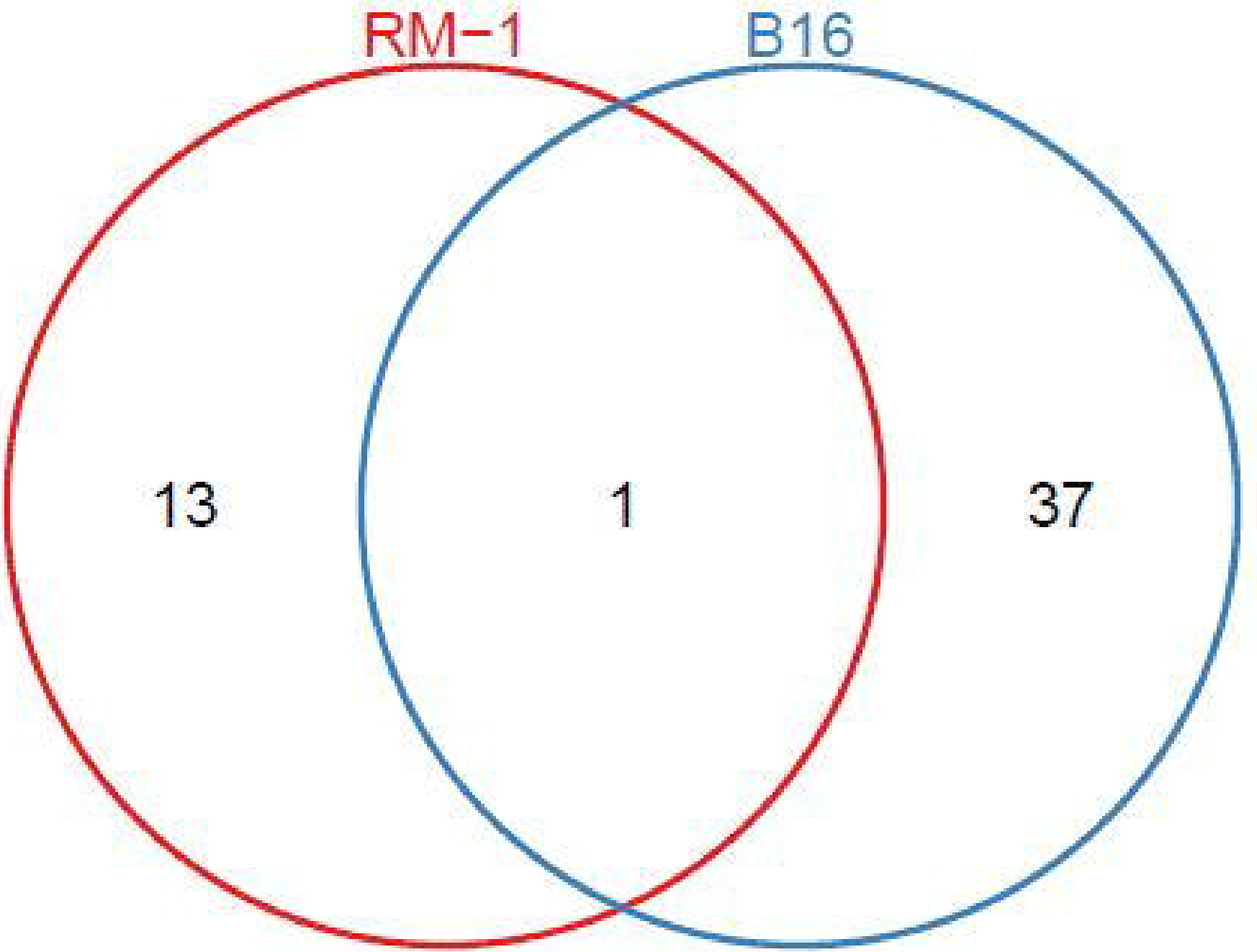
RM-1
B16
13
1
37

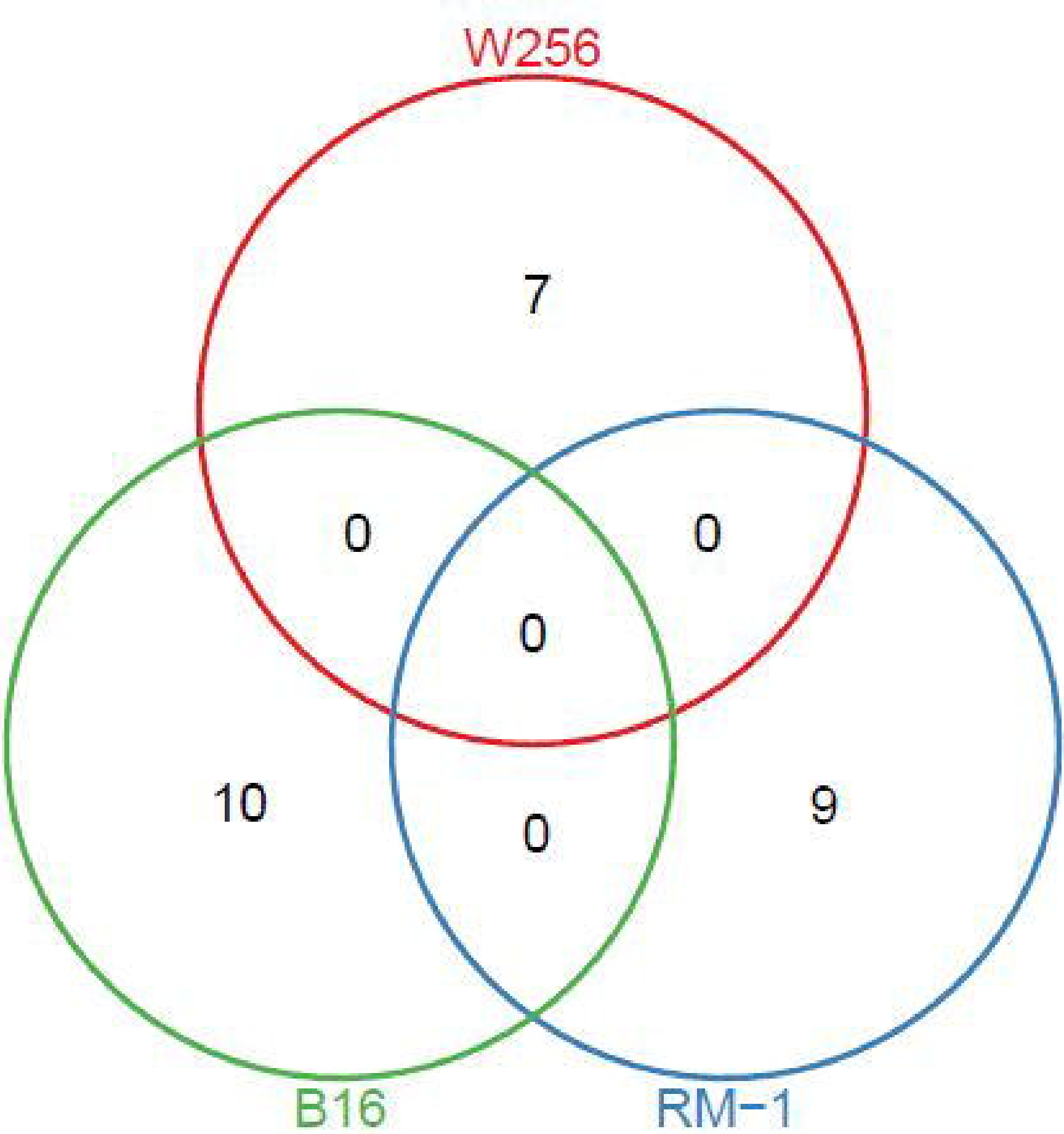
W256
7
0
0
0
10
0
9
B16
RM-1

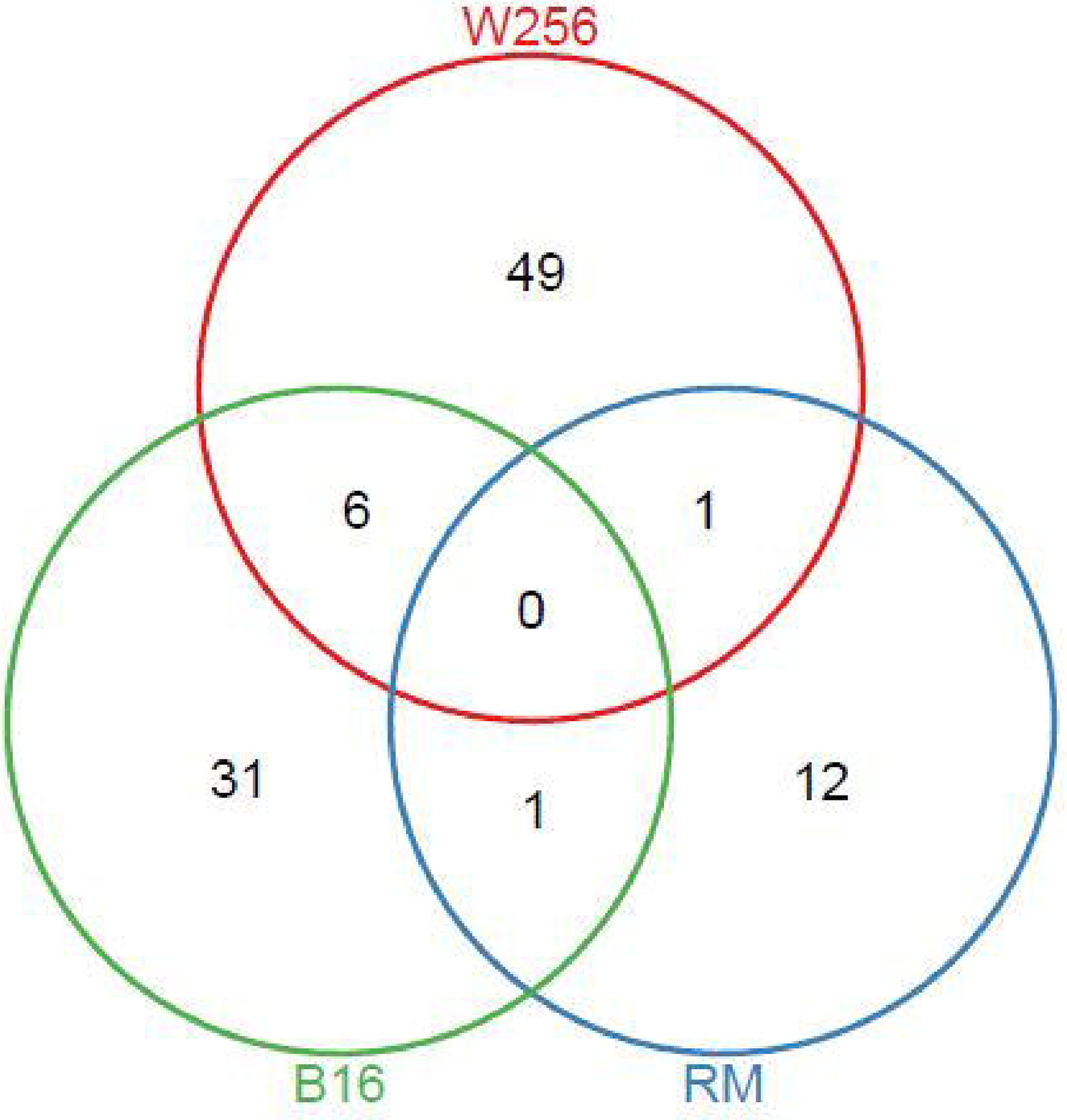
W256
49
6
1
0
31
1
12
B16
RM

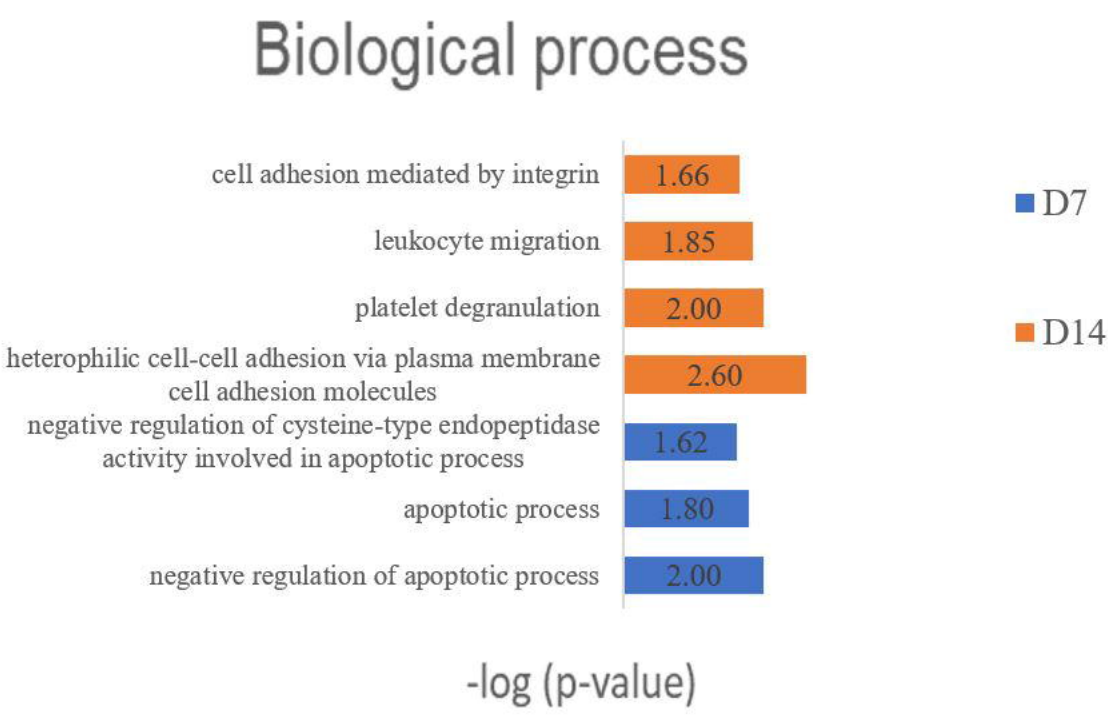
Biological process
cell adhesion mediated by integrin
1.66
leukocyte migration
1.85
platelet degranulation
2.00
heterophilic cell-cell adhesion via plasma membrane cell adhesion molecules
2.60
negative regulation of cysteine-type endopeptidase activity involved in apoptotic process
1.62
apoptotic process
1.80
negative regulation of apoptotic process
2.00
D7
D14
-log (p-value)

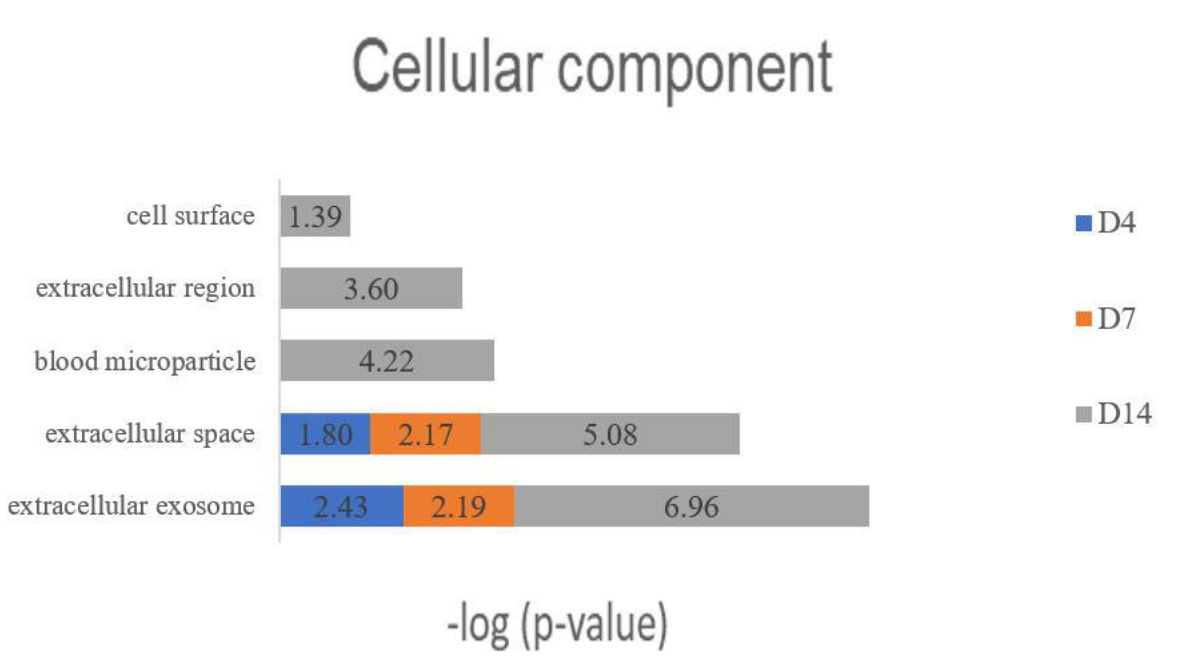
Cellular component
cell surface
extracellular region
blood microparticle
extracellular space
extracellular exosome
1.39
3.60
4.22
1.80
2.17
5.08
2.43
2.19
6.96
D4
D7
D14
-log (p-value)

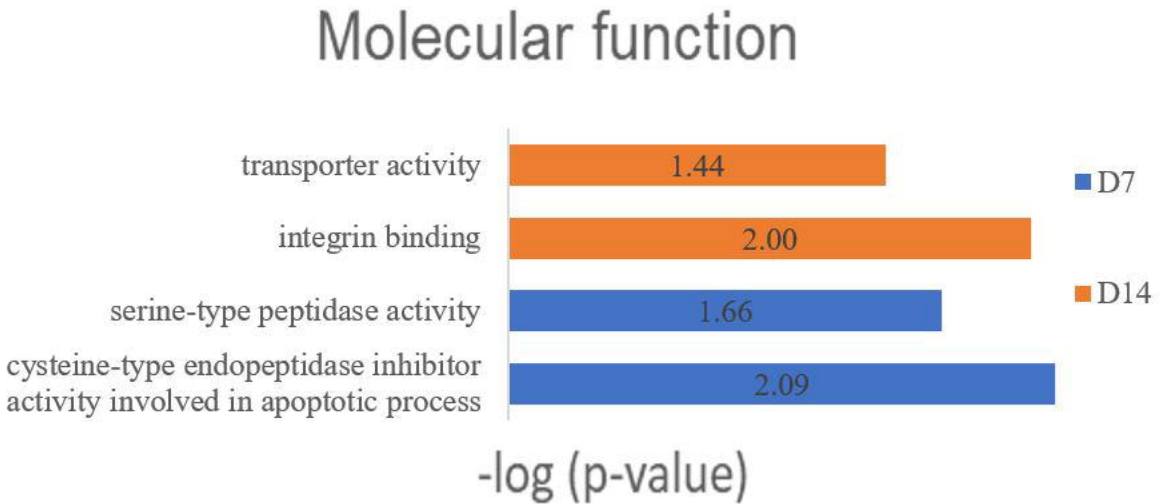
Molecular function
transporter activity
integrin binding
serine-type peptidase activity
cysteine-type endopeptidase inhibitor activity involved in apoptotic process
1.44
2.00
1.66
2.09
D7
D14
-log (p-value)

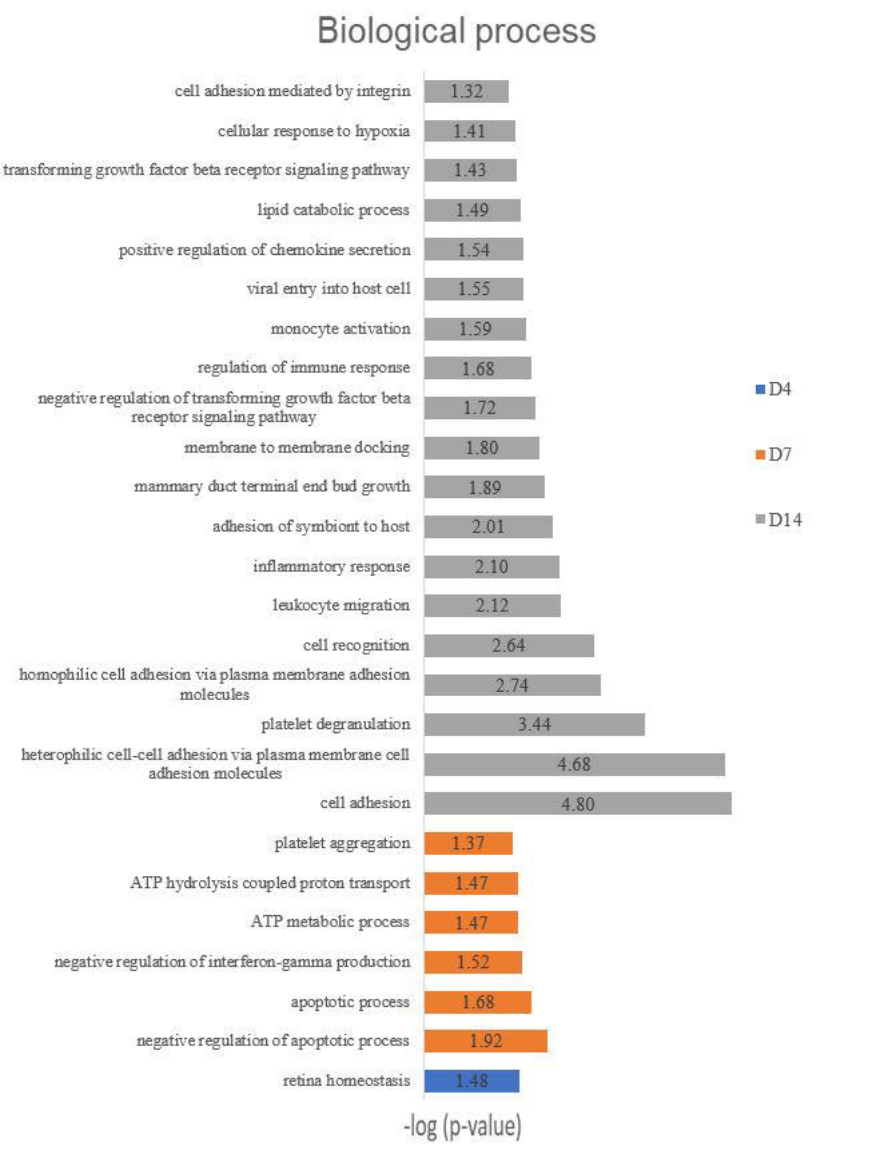
Biological process
cell adhesion mediated by integrin
1.32
cellular response to hypoxia
1.41
transforming growth factor beta receptor signaling pathway
1.43
lipid catabolic process
1.49
positive regulation of chemokine secretion
1.54
viral entry into host cell
1.55
monocyte activation
1.59
regulation of immune response
1.68
negative regulation of transforming growth factor beta receptor signaling pathway
1.72
membrane to membrane docking
1.80
mammary duct terminal end bud growth
1.89
adhesion of symbiont to host
2.01
inflammatory response
2.10
leukocyte migration
2.12
cell recognition
2.64
homophilic cell adhesion via plasma membrane adhesion molecules
2.74
platelet degranulation
3.44
heterophilic cell-cell adhesion via plasma membrane cell adhesion molecules
4.68
cell adhesion
4.80
platelet aggregation
1.37
ATP hydrolysis coupled proton transport
1.47
ATP metabolic process
1.47
negative regulation of interferon-gamma production
1.52
apoptotic process
1.68
negative regulation of apoptotic process
1.92
retina homeostasis
1.48
D4
D7
D14
-log (p-value)

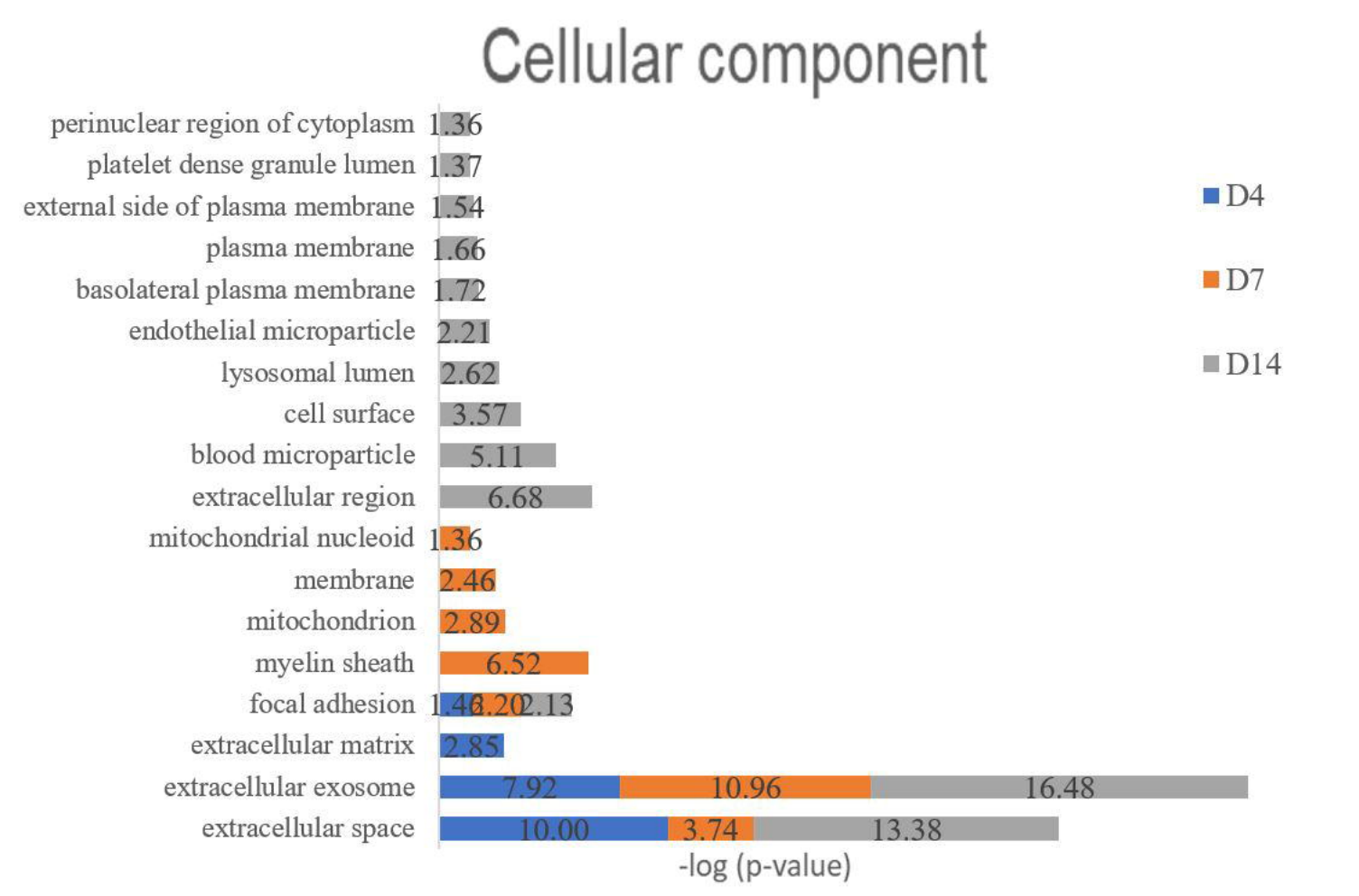
Cellular component
perinuclear region of cytoplasm
platelet dense granule lumen
external side of plasma membrane
plasma membrane
basolateral plasma membrane
endothelial microparticle
lysosomal lumen
cell surface
blood microparticle
extracellular region
mitochondrial nucleoid
membrane
mitochondrion
myelin sheath
focal adhesion
extracellular matrix
extracellular exosome
extracellular space
1.36
1.37
1.54
1.66
1.72
2.21
2.62
3.57
5.11
6.68
1.36
2.46
2.89
6.52
1.46
6.20
2.13
2.85
7.92
10.96
16.48
10.00
3.74
13.38
D4
D7
D14
-log (p-value)

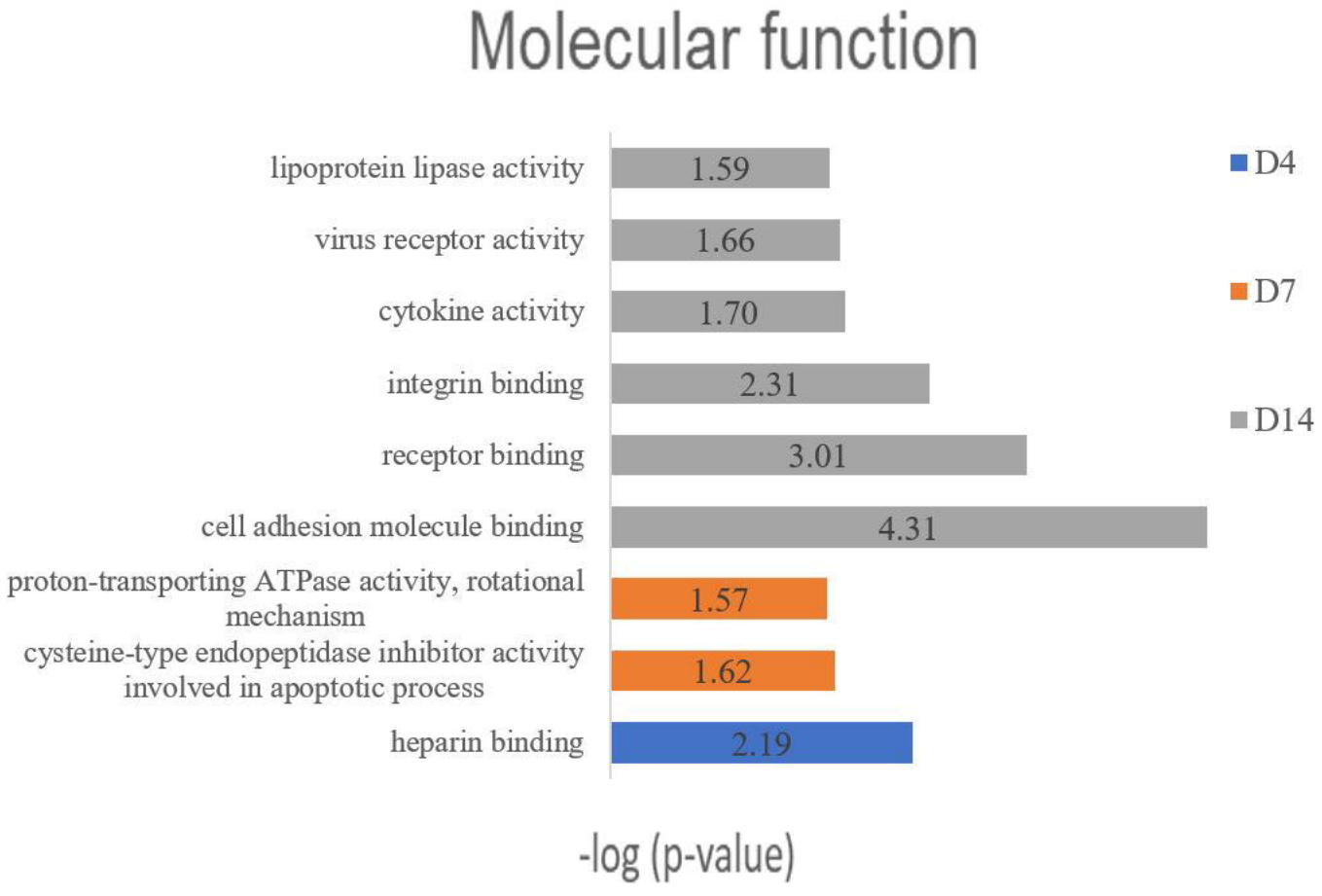
Molecular function
lipoprotein lipase activity
1.59
virus receptor activity
1.66
cytokine activity
1.70
integrin binding
2.31
receptor binding
3.01
cell adhesion molecule binding
4.31
proton-transporting ATPase activity, rotational mechanism
1.57
cysteine-type endopeptidase inhibitor activity involved in apoptotic process
1.62
heparin binding
2.19
D4
D7
D14
-log (p-value)

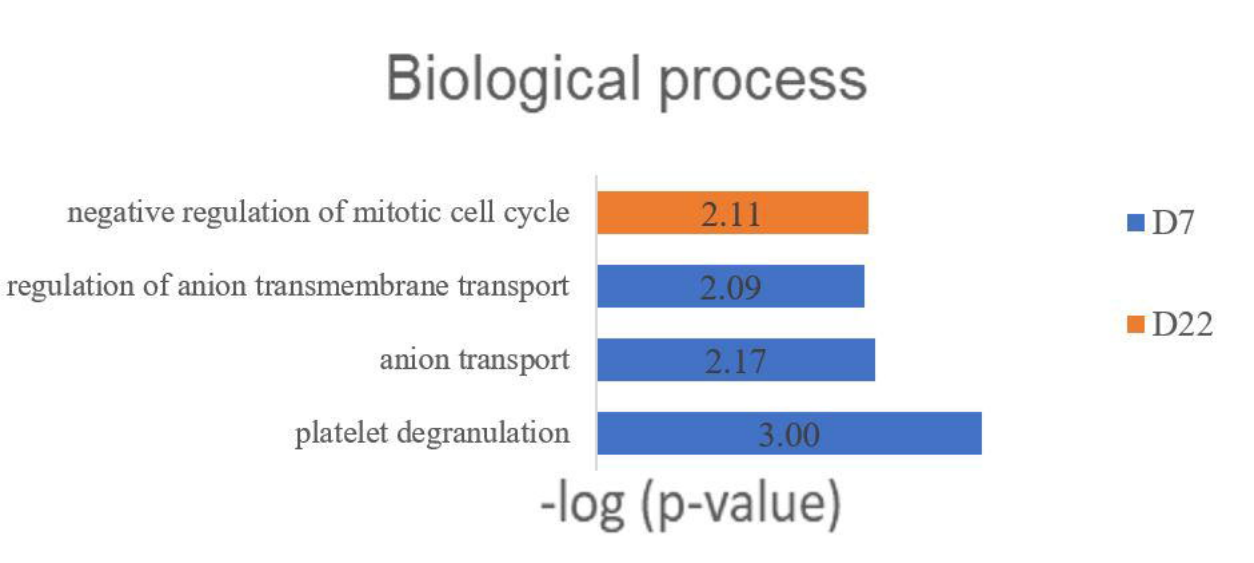
Biological process
negative regulation of mitotic cell cycle
regulation of anion transmembrane transport
anion transport
platelet degranulation
2.11
2.09
2.17
3.00
D7
D22
-log (p-value)

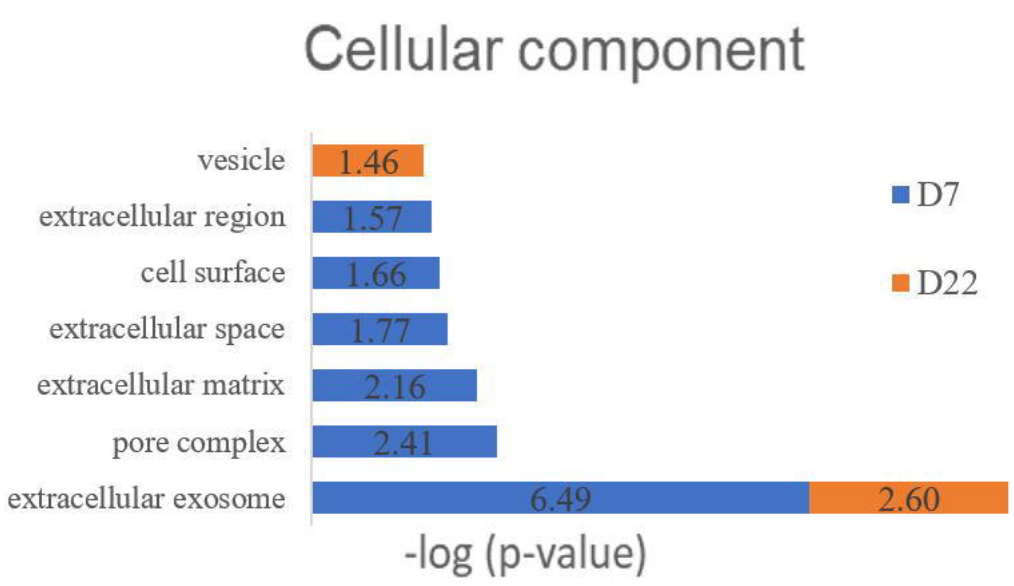
Cellular component
vesicle
extracellular region
cell surface
extracellular space
extracellular matrix
pore complex
extracellular exosome
1.46
1.57
1.66
1.77
2.16
2.41
6.49
2.60
D7
D22
-log (p-value)

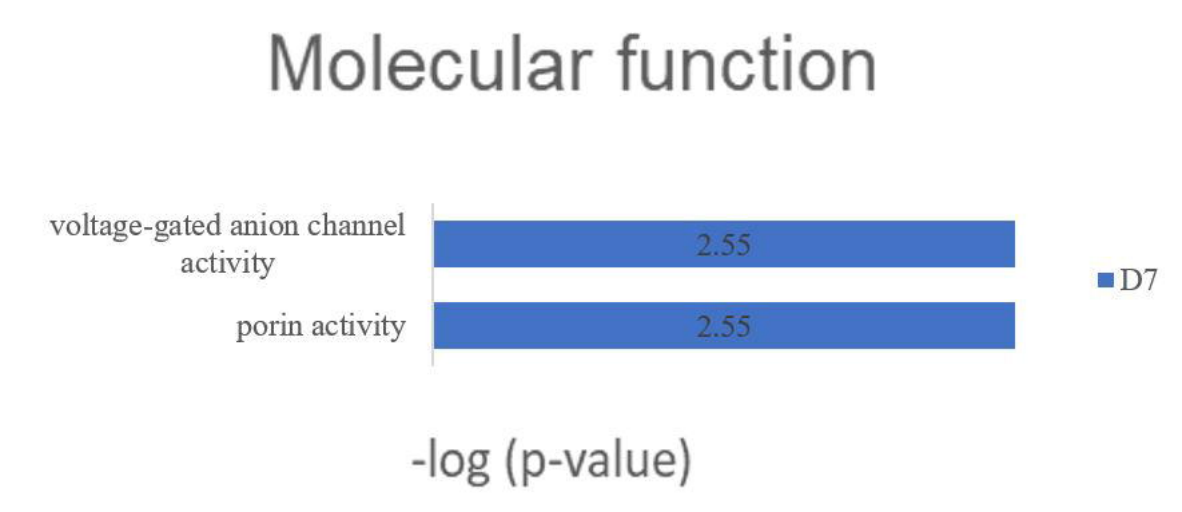
Molecular function
voltage-gated anion channel activity
porin activity
2.55
2.55
D7
-log (p-value)

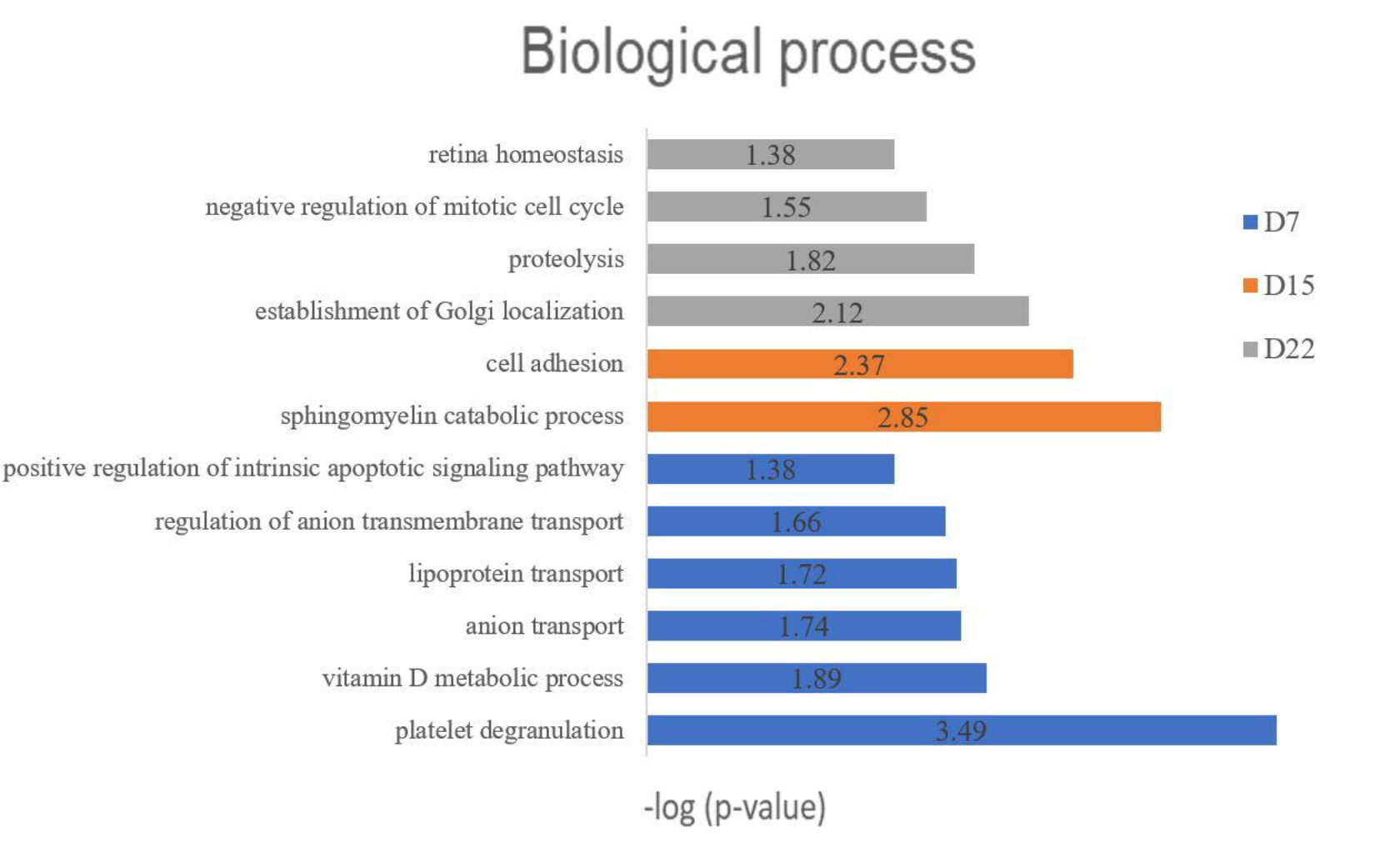
Biological process
retina homeostasis
negative regulation of mitotic cell cycle
proteolysis
establishment of Golgi localization
cell adhesion
sphingomyelin catabolic process
positive regulation of intrinsic apoptotic signaling pathway
regulation of anion transmembrane transport
lipoprotein transport
anion transport
vitamin D metabolic process
platelet degranulation
1.38
1.55
1.82
2.12
2.37
2.85
1.38
1.66
1.72
1.74
1.89
3.49
D7
D15
D22
-log (p-value)

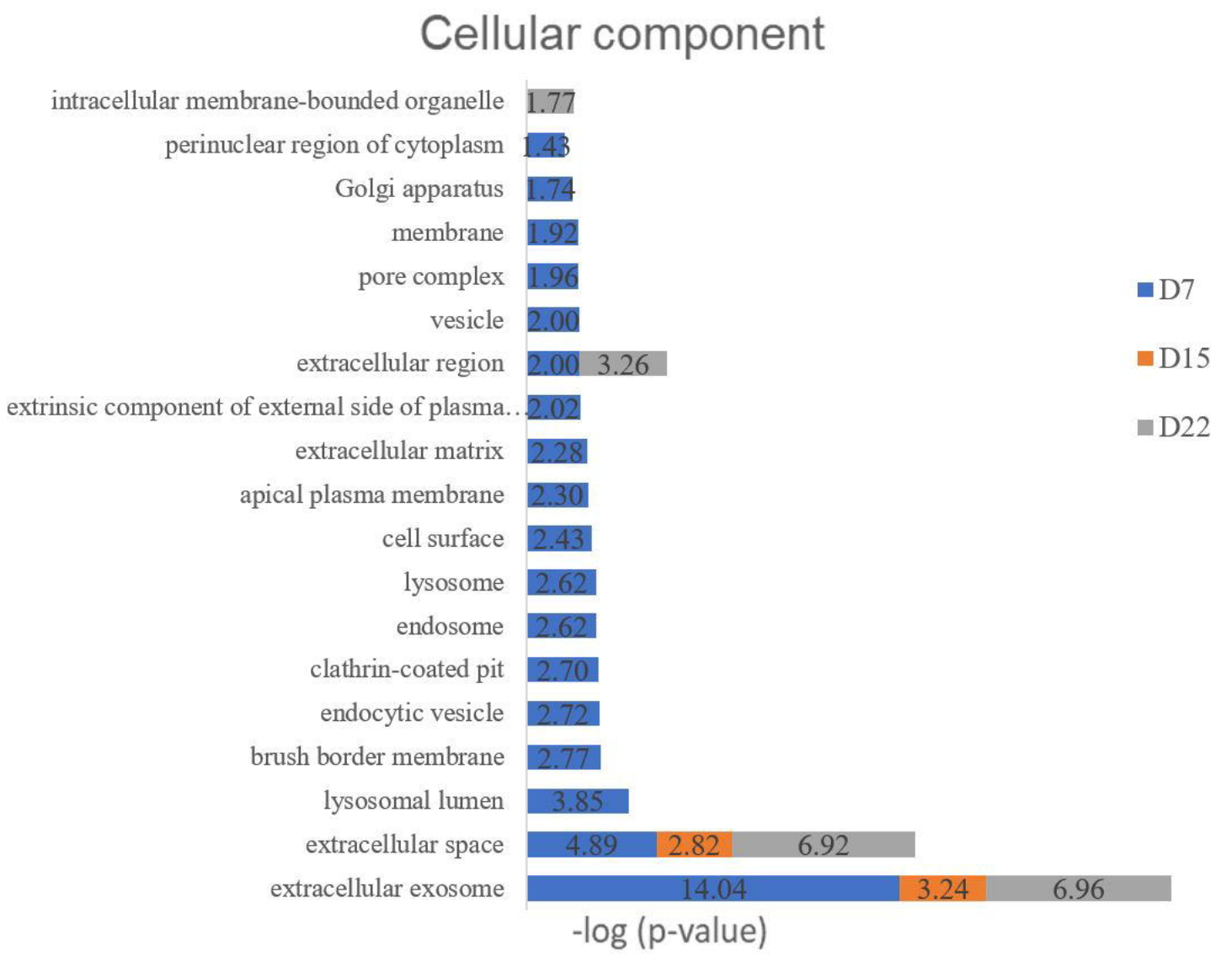
Cellular component
intracellular membrane-bounded organelle
perinuclear region of cytoplasm
Golgi apparatus
membrane
pore complex
vesicle
extracellular region
extrinsic component of external side of plasma…
extracellular matrix
apical plasma membrane
cell surface
lysosome
endosome
clathrin-coated pit
endocytic vesicle
brush border membrane
lysosomal lumen
extracellular space
extracellular exosome
1.77
1.43
1.74
1.92
1.96
2.00
2.00
3.26
2.02
2.28
2.30
2.43
2.62
2.62
2.70
2.72
2.77
3.85
4.89
2.82
6.92
14.04
3.24
6.96
D7
D15
D22
-log (p-value)

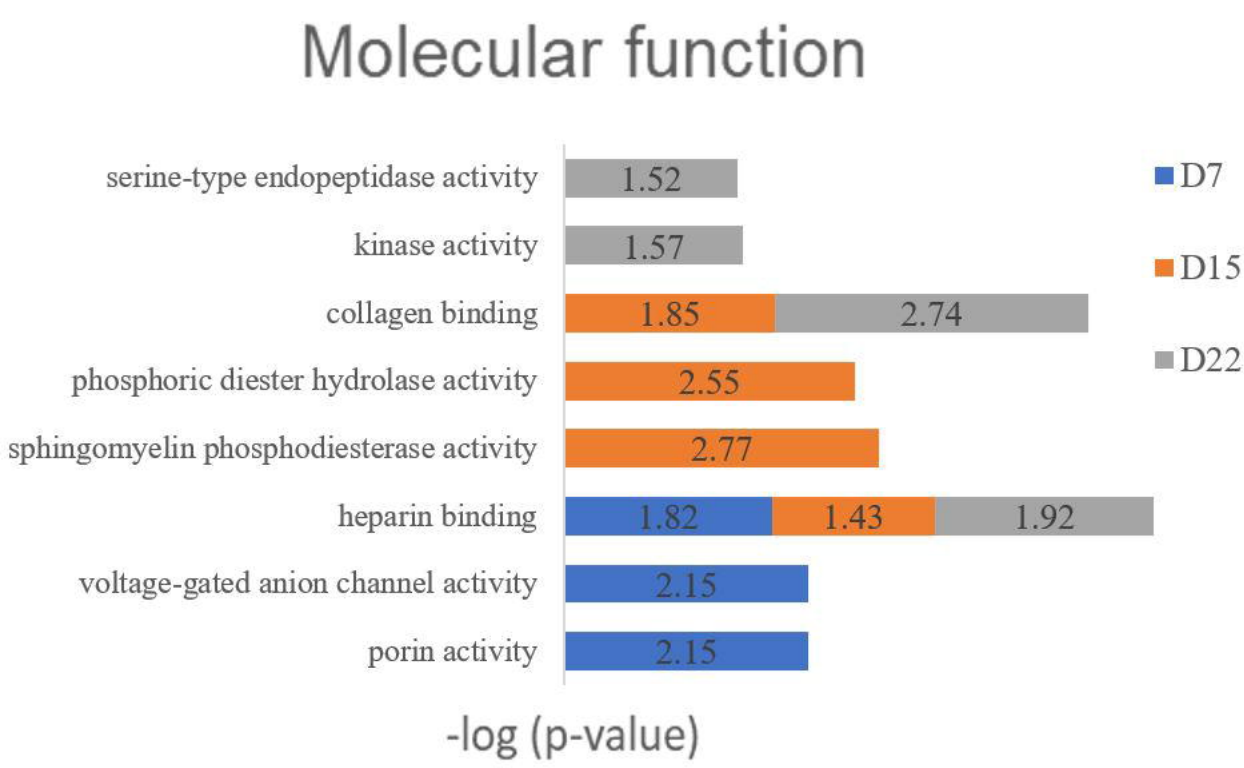
Molecular function
serine-type endopeptidase activity
kinase activity
collagen binding
phosphoric diester hydrolase activity
sphingomyelin phosphodiesterase activity
heparin binding
voltage-gated anion channel activity
porin activity
1.52
1.57
1.85
2.74
2.55
2.77
1.82
1.43
1.92
2.15
2.15
D7
D15
D22
-log (p-value)